Ligand requirements for immunoreceptor triggering

Michael I. Barton, Rachel L. Paterson[1], Eleanor M. Denham[2], Jesse Goyette[3,4], P. Anton van der van der Merwe[4,5]

Sir William Dunn School of Pathology, University of Oxford, Oxford OX1 3RE

[1]Current address: Stemmatters, Biotecnologia e Medicina Regenerativa SA, Parque de Ciência e Tecnologia Avepark, Zona Industrial da Gandra, Barco, Portugal

[2]Current address: Enara Bio, The Magdalen Centre, Oxford Science Park, 1 Robert Robinson Avenue, Oxford OX4 4GA

[3]Current address: Department of Molecular Medicine, School of Biomedical Sciences, University of New South Wales, Sydney 2052, NSW, Australia

[4]These authors contributed equally

[5]Correspondence: anton.vandermerwe@path.ox.ac.uk

Abstract

Leukocytes interact with other cells using cell surface receptors. The largest group of such receptors are non-catalytic tyrosine phosphorylated receptors (NTRs), also called immunoreceptors. NTR signalling requires phosphorylation of cytoplasmic tyrosine residues by SRC-family tyrosine kinases. How ligand binding to NTRs induces this phosphorylation, also called NTR triggering, remains controversial, with roles suggested for size-based segregation, clustering, and mechanical force. Here we exploit a recently developed cell-surface generic ligand system to explore the ligand requirements for NTR triggering. We examine the effect of varying the ligand's length, mobility and valency on the activation of representative members of four NTR families: SIRPβ1, Siglec 14, NKp44 and TREM-1. Increasing the ligand length impairs activation via NTRs, despite enhancing cell-cell conjugation, while varying ligand mobility has little effect on either conjugation or activation. Increasing the valency of the ligand, while enhancing cell-cell conjugation, does not enhance activation at equivalent levels of conjugation. These findings support a role for size-based segregation, rather than mechanical force or clustering, in NTR triggering, consistent with the kinetic-segregation model.

Introduction

The cell surface of an immune cell or leukocyte presents many different receptors, which sense their environment through ligand binding (Barclay et al., 1997; Shilts et al., 2022; Springer, 1990). Many leukocyte receptors bind to ligands on the surface of other cells to mediate adhesion and/or transduce signals which regulate leukocyte function. These signals determine whether the leukocyte ignores or responds to the cell and influence the nature of the response. The largest class of such receptors are non-catalytic tyrosine-phosphorylated receptors (NTRs), which are also called immunoreceptors (Dushek et al., 2012). More than one hundred leukocyte receptors, in more than 20 families, can be classified as NTRs (Dushek et al., 2012). Because they regulate immune cell function, NTRs have roles in a wide range of diseases, and they are being exploited for therapeutic purposes. For example, synthetic NTRs (e.g. chimeric antigen receptors) and antibodies targeting NTRs or their ligands (e.g. checkpoint inhibitors) have become standard therapies for several forms of cancer (June and Sadelain, 2018; Sharma and Allison, 2015).

While NTRs have structurally diverse extracellular regions they all have, or are associated with signalling subunits that have, conserved tyrosine containing motifs in their cytoplasmic domains, such as the immunoreceptor tyrosine-based activation motif (ITAM) and immunoreceptor tyrosine-based switch motif (ITSM) (Dushek et al., 2012). These motifs are phosphorylated by SRC-family tyrosine kinases, which are tethered via acyl groups to the inner leaflet of the plasma membrane. This phosphorylation is

49 regulated by the receptor tyrosine phosphatases CD45 and CD148, which act on both SRC-kinases and
50 their substrates. While the extracellular regions of NTRs are structurally diverse, they are typically
51 smaller (4-10 nm) than many abundant cell surface molecules such as CD43, CD44, CD45, CD148 and
52 integrins, which range in size from 21-50 nm. When these size differences were first noted for the TCR
53 and its peptide-MHC (pMHC) ligand it was predicted that, when T cells contacted other cells, there
54 would be segregation of the TCR/pMHC complex from larger molecules like CD45 (Springer, 1990). This
55 observation, together with evidence that constitutive tyrosine phosphatase activity suppresses TCR
56 triggering in resting cells (O'Shea et al., 1992; Secrist et al., 1993), led to the proposal that TCR binding
57 to pMHC induced tyrosine phosphorylation of the TCR by trapping it in small regions of close contact
58 which exclude large receptor tyrosine phosphatases CD45 and CD148 but not the SRC-kinases (Davis and
59 van der Merwe, 1996). This mechanism was subsequently termed the kinetic segregation (KS) model
60 (van der Merwe et al., 2000). Subsequent studies from multiple laboratories using a wide range of
61 techniques have demonstrated that the KS mechanism plays a key role in TCR triggering (Burroughs et
62 al., 2006; Chang et al., 2016; Chen et al., 2021; Choudhuri et al., 2005; Cordoba et al., 2013; James and
63 Vale, 2012; Jenkins et al., 2023; Razvag et al., 2018; Schmid et al., 2016; Varma et al., 2006; Wilhelm et
64 al., 2021). Recently it has been shown that synthetic receptors based on the TCR, namely chimeric
65 antigen receptors (CARs), also appear to trigger by the KS mechanism, which has important implications
66 for the design of these receptors and selection of their target antigens (Xiao et al., 2022). Other
67 mechanisms that been proposed to contribute to TCR triggering are aggregation (Goyette et al., 2019) or
68 conformational change, with conformational change being either allosteric (Schamel et al., 2019) or
69 induced by mechanical force (Ma et al., 2008; Zhu et al., 2019).

70 The similarities in signalling between the TCR and other NTRs have led to the hypothesis that the KS
71 mechanism may contribute to triggering by other NTRs (Davis and van der Merwe, 2006; Dushek et al.,
72 2012). Indeed, evidence for this has been reported for NKG2D in NK cells (Köhler et al., 2010), Dectin-1
73 (Goodridge et al., 2011) and FcyRs (Bakalar et al., 2018) in macrophages, and CD28 in T cells (Lim et al.,
74 2015). However, the diversity of NTRs and their ligands, and the fact that many NTR ligands have yet to
75 be identified, has hampered investigation of the triggering mechanism in a wider range of NTRs. We
76 have recently developed a generic ligand system based on the SpyTag/SpyCatcher split protein, which
77 enables cell-surface Streptactin to be used to engage any NTR incorporating a membrane-distal
78 StrepTagII peptide (Denham et al., 2019). Importantly, this generic ligand stimulated TCRs at the same
79 surface density as the native TCR ligand, validating it as a suitable model system for investigating NTR
80 triggering (Denham et al., 2019).

81 In the present study we used this generic ligand system to explore the ligand requirement for triggering
82 by representative members of 4 distinct NTR families (Figure 1A): Signal regulatory protein β1 (SIRPβ1),

83 Sialic acid-binding immunoglobulin-type lectin 14 (Siglec 14), Natural killer receptor 44 (NKp44) and
84 Triggering receptor expressed on myeloid cells 1 (TREM-1). SIRPβ1 is highly homologous to the
85 inhibitory receptor and therapeutic target SIRPα (Kharitonenkov *et al.*, 1997). SIRPβ1 and SIRPα are
86 examples of paired activatory/inhibitory NTRs (Dushek et al., 2012), with conserved extracellular regions
87 but distinct transmembrane and cytoplasmic domains. The native ligand of SIRPβ1 is unknown but it is
88 thought to promote phagocytosis in macrophages (Hayashi *et al.*, 2004). Siglec 14 is a member of the
89 sialic acid-binding Siglec family of receptors (Angata et al., 2006; Crocker et al., 2007). Siglec 14 and
90 Siglec 5 are paired activatory and inhibitory NTRs, respectively (Angata *et al.*, 2006). NKp44 is important
91 for the activation and cytotoxic activity of natural killer cells and reportedly binds a wide range of ligands
92 (Parodi et al., 2019). Finally, TREM-1 is an activatory member of a family of NTRs (Ford and McVicar,
93 2009) that has been reported to bind peptidoglycan recognition protein 1 (PGLYRP1) (Read *et al.*, 2015)
94 and extracellular actin (Fu *et al.*, 2017). All four receptors associate with, and presumably signal using,
95 the ITAM-containing adaptor protein DAP12 (Lanier and Bakker, 2000).

96 To investigate the triggering mechanism used by these NTRs we examined the effect of changing ligand
97 size, mobility, and valency on activation. Elongating the ligand inhibited activation via these receptors
98 despite enhancing receptor/ligand mediated cell-cell conjugation. In contrast, changing the ligand
99 mobility had little effect on conjugation or activation. Finally, while increasing the ligand valency
100 increased cell-cell conjugation as well as activation, it decreased the level of activation at equivalent
101 levels of cell-cell conjugation. Taken together, these results support a role for the KS mechanism in
102 triggering by these NTRs, and argue against roles for mechanical force or clustering.

103 Results

104 Varying ligand length

105 In the SpyTag-SpyCatcher system a covalent (isopeptide) bond spontaneously forms between Spytag
106 and SpyCatcher when they are mixed together (Zakeri *et al.*, 2012). In our previously described generic
107 ligand system (Denham et al., 2019), SpyTag is fused to the N-terminus of a transmembrane protein
108 expressed on ligand-presenting CHO cells, forming the ligand anchor, while SpyCatcher is fused to a
109 Strep-Tactin tetramer, which can have from one to four active binding sites, as required (Figure 1A). The
110 receptor is modified at its membrane-distal N-terminus to contain a Strep-tag II peptide, which binds
111 monovalent Strep-Tactin with a K_D of 43 μM (Denham et al., 2019). This is within the affinity range
112 typical of leukocyte cell-cell interactions (van der Merwe and Barclay, 1994; Shilts et al., 2022).

113 To test the effect of ligand length on activation via NTRs, we produced CHO cells expressing either a
114 short or a long ligand anchor, where the latter includes a ~11 nm spacer comprising the four Ig domains

115 of CD4 (Figure 1A) (Wu et al., 1997). By titrating the monovalent Strep-Tactin SpyCatcher we produced a
116 panel of CHO cells with a range of binding sites. We used a previously described method to accurately
117 quantify the number of Strep-Tactin binding sites presented by these cells (Denham et al., 2019). This
118 involved measuring the maximum number of biotin binding sites and the K_D for Strep-Tactin SpyCatcher
119 coupling to cells (sFigure 1) and using these parameters to calculate the number of binding sites, as
120 described in the Materials and Methods.

121 We first measured the impact of ligand elongation on the receptor engagement using a cell-cell
122 conjugation assay as a readout. For receptor cells we used monocytoid THP-1 cells expressing the
123 SIRPβ1 receptor with an N-terminal Strep-tag II peptide. The conjugation assay involves mixing receptor
124 and ligand cells stained with different fluorescent dyes and measuring double positive events by flow
125 cytometry (Figure 1B, upper right quadrants). As expected, reducing the number of binding sites
126 resulted in a decrease in the percentage of receptor cells in conjugates (Figure 1B).

127 We then compared the conjugation efficacy of SIRPβ1 THP-1 cells mixed with short or long CHO cells
128 presenting different numbers of binding sites. When plotting conjugates against binding sites, cells
129 presenting the long ligand produced more conjugates (Figure 1C, left panel). This suggests that
130 increasing the ligand length promotes conjugate formation, which is consistent with other studies
131 suggesting that increasing the length of short (< 8 nm) cell surface ligands improves receptor
132 engagement (Choudhuri et al., 2005; Lim et al., 2015; Wild et al., 1999).

133 We next examined the effect of ligand length on SIRPβ1 mediated IL-8 production. Interestingly the
134 long ligand stimulated less IL-8 production than the short ligand (Figure. 1C, middle panel), despite
135 mediating improved conjugate formation. To normalise for differences in conjugate formation we
136 plotted the functional IL-8 response against the percentage of receptor cells in conjugates (Figure 1C,
137 right panel). This confirmed that, at equivalent levels of conjugate formation, the long ligand induced
138 lower levels of IL-8 production.

139 We performed conjugation and stimulation assays on other NTRs (Siglec 14, NKp44 and TREM-1) using
140 the short or long generic ligand (Figure 2). As in the case of SIRPβ1, the results for NKp44 and TREM-1
141 show an increase in conjugation efficacy when binding to the long ligand compared to the short ligand
142 (Figure 2, left panels). This was not the case for Siglec 14, where no difference was seen (Figure 2B, left
143 panel). Elongation of the ligand impaired activation of IL-8 release via all four NTRs, both before and
144 after normalising for conjugate formation (Figure 2, centre and right panels, respectively).

145 One likely explanation for the effect of ligand length on activation efficiency is that increasing the ligand
146 length increases the length of the NTR/ligand complex. If this is the case, activation should also be

147 reduced by increasing the length of the NTRs. The extracellular regions of SIRPβ1 and Siglec 14 each
148 contain 3 immunoglobulin superfamily (IgSF) domains, whereas the extracellular regions of NKp44 and
149 TREM-1 only have 1 IgSF domain (Figure 1A). To examine whether this size difference had a measurable
150 impact we reanalysed the data in Figure 2 to enable comparison of conjugation and activation via NTRs
151 exposed to the same ligand (sFigure 3). Short NTRs (NKp44 and TREM-1) mediated lower levels of
152 conjugation (sFigure 3, left panels) but high levels of stimulation when normalised for conjugation
153 (sFigure 3, right panels), and this was observed with both short (sFigure 3A) and long (sFigure 3B)
154 ligands. Taken together, these data show that elongation of these NTR/ligand complexes attentuates
155 activation via these four NTRs.

156 **Varying ligand mobility**

157 We next examined the effect of varying the ligand anchor on NTR activation. We compared ligand
158 anchors based on the transmembrane and cytoplasmic domains of CD80, and CD43 and the
159 glycosylphosphatidylinositol (GPI) anchor of CD52. The CD43 cytoplasmic domain interacts with the actin
160 cytoskeleton though Ezrin/Radixin/Moesin (ERM) proteins (Yonemura *et al.*, 1998), and so is likely to be
161 more firmly anchored. In contrast, CD52 is a GPI anchored protein and thus less firmly anchored, and
162 presumably more mobile (Figure 3A). To examine mobility, SpyCatcher-GFP was coupled to ligand
163 anchors and fluorescence recovery after photobleaching (FRAP) performed. As expected, the CD52
164 anchor conferred greater mobility than the CD80 or CD43 anchor, which were similar (Figure 3B).

165 We next compared the effect of changing the ligand mobility on conjugation with and stimulation of
166 SIRPβ1 expressing THP-1 cells. It was not possible to attain as high a level of binding sites on the CD43
167 and CD52 ligand anchor cells but comparison was possible over a reasonable range. CD52 and CD43
168 anchored ligands induced similar levels of conjugate formation (Figure 3C, top panel) and IL-8 release
169 (Figure 3C, middle panel) at comparable levels of binding sites. CD52 anchored ligand induced slightly
170 less IL-8 release than CD43 anchored ligands when plotted against levels of conjugation (Figure 3C,
171 bottom panel). However this difference was small and could be the result of faster turnover of the CD52
172 anchored ligand (sFigure 5), which would reduce engagement during the 20 h stimulation. While the
173 CD80 anchored ligand was less potent at mediating conjugation and IL-8 release, this was not a
174 consequence of differences in lateral mobility which was similar to the lateral mobility of the CD43
175 anchored ligand (Figure 3B). Taken together, these results suggest that changes in the ligand mobility do
176 not affect SIRPβ1 mediated conjugation or triggering.

177 **Varying ligand valency**

178 Since ligand-induced clustering of receptors is often assumed to be the mechanism of receptor-
179 activation, we next examined the effect of increasing the valency of the ligand from 1 to 4 by using a
180 tetravalent form of Strep-Tactin Spycatcher. As expected, conjugation with tetravalent instead of
181 monovalent Strep-Tactin Spycatcher resulted in a four-fold increase in the number of binding sites
182 (sFigure 6). We then compared the ability of monovalent and tetravalent ligand to mediate conjugation
183 and induce IL-8 secretion from THP-1 cells expressing the 4 different NTRs. Tetravalent ligand induced
184 conjugation via all 4 NTRs at lower ligand binding site numbers than monovalent ligand (Figure 4, left
185 panels), indicating that increasing the ligand valency increases NTR binding, presumably by increasing
186 avidity. Increasing the valency enabled activation of all four receptors, as measured by IL-8 release, at
187 much lower ligand binding sites (Figure 4, middle panels). However, after controlling for increased
188 conjugate formation, tetravalent ligand was actually less effective than monovalent ligand at stimulating
189 IL-8 release at equivalent levels of conjugation (Figure 4, right panels). The same result was observed
190 with the CD80, CD43 and CD52 ligand anchors (sFigure 7 and 8). These results indicate that, while
191 increasing the valency of a cell surface-associated ligand enhances binding to NTRs, it does not increase
192 activation via NTRs.

193 We next investigated whether activation of NTR by the high avidity tetravalent Strep-Tactin SpyCatcher
194 was sensitive to ligand length. THP-1 cells expressing four representative NTRs were exposed to CHO
195 cells presenting tetravalent Strep-Tactin SpyCatcher on either short or long CD80 anchors (Figure 5). The
196 short ligands were less effective at mediating conjugation than the long ligand for two (SIRPβ1 & NKp44)
197 of the four NTRs (Figure 5, left panels), but more effective at stimulating IL-8 production for three of the
198 four NTRs (SIRPβ1, NKp44 and TREM-1), both before (Figure 5, centre panels) and after (Figure 5, right
199 panels) controlling for conjugate formation. These results show that even high avidity NTR/ligand
200 interactions remain sensitive to ligand length for three of the four NTRs studied here.

201 ## Discussion

202 We have exploited our previously described generic cell surface ligand system (Denham et al., 2019) to
203 explore the effects of varying ligand length, mobility, and valency on activation of four representative
204 NTRs, SIRPβ1, Siglec-14, NKp44 and TREM-1. One advantage of this system is that it enables titration of
205 ligand surface density, enabling detection of quantitative differences in the ability of cell-surface ligands
206 to mediate conjugation and stimulation. A second advantage is that it enables multiple NTRs to be
207 assessed using the same set of ligands, increasing throughput and facilitating comparisons between
208 NTRs. A third advantage is that it enables analysis of orphan NTRs, such as SIRPβ1, whose ligands have
209 yet to be identified.

210 Our first key finding is that elongation of generic ligands abrogated activation of all four NTRs. This was
211 not a consequence of decreased binding as elongated ligands mediate enhanced cell-cell conjugation.
212 While this contrasted with results in a supported lipid bilayer (SLB) system, in which elongation of CD48
213 abrogated CD2 binding (Milstein et al., 2008), it is consistent with results obtained with cell surface
214 expressed ligands, including CD48 (Choudhuri et al., 2005; Köhler et al., 2010; Lim et al., 2015; Wild et
215 al., 1999). A likely explanation for this is that ligands on cell surfaces, unlike ligands on SLBs, are crowded
216 by the larger molecules present at high densities. Our finding that long NTRs were less effectively
217 activated than short NTRs suggest that the increased NTR/ligand length abrogates NTR signalling. These
218 data are most consistent with the KS mechanism of NTR triggering (Davis and van der Merwe, 2006),
219 since increasing the NTR/ligand length would be expected to increase the intermembrane distance and
220 thus reduce segregation of inhibitory receptor tyrosine phosphatases such as CD45 from the engaged
221 NTR (Choudhuri et al., 2005). Numerous studies have confirmed that increasing receptor/ligand length
222 abrogates CD45 segregation from engaged NTRs (Al-Aghbar et al., 2018; Bakalar et al., 2018; Chen et al.,
223 2017; Choudhuri et al., 2005; Lim et al., 2015; Xiao et al., 2022). In one of these studies an elongated
224 high affinity TCR ligand, derived from the OKT3 monoclonal antibody, was able to activate TCRs despite
225 less efficient exclusion of CD45 (Al-Aghbar et al., 2018). However, no titration of the ligand number was
226 performed, and a lower affinity variant of the same ligand was unable to activate T cells (Al-Aghbar et
227 al., 2018).

228 An alternative explanation for our finding that elongation abrogates activation through NTRs is that this
229 could decrease the level of force experienced by the NTR upon ligand engagement (Li et al., 2010).
230 These data are therefore also consistent with models of NTR triggering postulating that a mechanical
231 force imposed upon ligand binding alters the conformation of the NTR (Ma et al., 2008; Zhu et al., 2019).
232 However, whether changing ligand length affects the force experienced by an NTR has yet to be
233 confirmed, and it remains unclear how such a conformational change of NTRs could be transmitted
234 through the membrane to enhance phosphorylation of their cytoplasmic domains. Such a mechanism is
235 difficult to reconcile with enormous structural variability of NTRs (Dushek et al., 2012) and the fact that
236 chimeric NTRs such as CARs tolerate extensive variation in the regions (hinge, transmembrane and
237 cytoplasmic domains) that couple their ligand binding domains with their tyrosine-containing signalling
238 motifs (Labanieh and Mackall, 2023; Sadelain, 2016).

239 A second key finding is that changing the mobility of the ligand anchor had little impact on its ability
240 mediate activation via NTRs. The CD52 anchor comprises a lipid (GPI) which we show confers greater
241 lateral mobility. A lipid anchor also allows a ligand to be more easily extracted from the plasma
242 membrane by force. Thus, the amount of force that can be exerted on an NTR, both tangential and
243 perpendicular to the membrane, should be lower with lipid-anchored than a transmembrane-anchored

244 ligand. Furthermore, CD43 is potentially able to bind to the actin cytoskeleton through ERM proteins,
245 which would further increase the force that can be exerted before the ligand is extracted from the cell
246 surface. Thus, our finding that CD43 and CD52 anchors were similarly effective at activating an NTR
247 argues against a substantial role for mechanical force in NTR triggering. In support of this, changing the
248 lateral mobility of the TCR ligand in an SLB system had no effect on TCR triggering despite substantially
249 changing the force experienced by the TCR (Göhring et al., 2021).

250 The third key finding is that increasing the valency of the NTR ligand did not increase activation of the
251 NTR at equivalent levels of cell-cell conjugation. This result contrasts with the findings obtained with
252 soluble NTR ligands such as cross-linked antibodies and natural ligands engineered to be multivalent,
253 where increasing the valency is required for NTR triggering (Boniface et al., 1998; Cochran et al., 2000).
254 One possible explanation for this discrepancy between the effect of valency with soluble and surface
255 associated ligand is that a soluble multivalent ligand could, by forming clusters of NTRs, exclude
256 molecules with bulky ectodomain, such as CD45, from clustered NTRs, whereas soluble monovalent
257 ligands are unable to do this. In contrast, even a monovalent surface-associated ligand can trap the NTR
258 in zones of a close intermembrane contact from which CD45 and CD148 are excluded. While our finding
259 that tetravalent ligands are less effective at activating NTRs than monovalent ligands requires
260 confirmation and further analysis, the fact that increased valency does not enhance NTR triggering is
261 strong evidence against aggregation as a mechanism of physiological NTR triggering. Further evidence
262 against this model is that almost all cell surface NTRs ligands that have been identified to date are
263 monovalent (Dushek et al., 2012). In contrast, cell surface receptors known to signal by binding induced
264 multimerisation, such as class III tyrosine kinase receptors (Ullrich and Schlessinger, 1990) and TNF
265 receptor superfamily members (Locksley et al., 2001), typically have multivalent ligands.

266 Our finding that elongation of a tetravalent generic ligand did not impair activation via Siglec 14, while it
267 did impair activation via the three other NTRs, suggests that, for some NTRs, increasing ligand valency
268 can bypass the need for the KS mechanism. It is noteworthy that some Siglec family members, including
269 the Siglec-14 paired receptor Siglec-5 (Cornish et al., 1998), are able to form disulphide linked dimers.
270 Dimeric Siglec-14 would allow formation of large 'zipper-like' aggregates with tetravalent generic ligand,
271 enabling exclusion of CD45 and CD148 without needing the KS mechanism.

272 Taken together, our finding that activation via NTRs is abrogated by ligand elongation and aggregation
273 and unaffected by the mobility of the ligand anchor supports our hypothesis that NTRs signal by the KS
274 mechanism. While our results focus only on four representative NTRs, these results are likely to apply to
275 a larger number of NTRs, including other members of the Siglec and TREM families and NTRs from other
276 families that signal via the DAP-12 adaptor (Lanier, 2008). As reviewed in the Introduction, there is

277 already evidence that many NTRs that do not associate with DAP12, including the TCR, NKG2D, CD28,
278 and FcγR, exploit the KS mechanism for triggering. Taken together with the results presented in this
279 paper, this demonstrates that the KS mechanism is used by NTRs which signal through intrinsic tyrosine
280 motifs (CD28, FcγRI and FcγRII) and a variety of signalling subunits (DAP12, DAP10, CD3δεγ, CD247, and
281 FcRγ).

282 One limitation of the present work is that we used artificial ligands rather than native ligands. Our
283 recent development of Combicells (Patel et al., 2023), which exploit the SpyCatcher/SpyTag system to
284 present native ligand on antigen presenting cells should enable our key results to be confirmed with
285 native ligands, where known. A second limitation, which is a consequence of the system used, is lack of
286 imaging data of the interface between THP-1 cells and CHO cells. Advanced microscopy, beyond the
287 scope of this study, is likely needed to image the molecular events in the microvilli-like structures and
288 close contact areas involved in NTR triggering at cell-cell interfaces (Jenkins et al., 2023; Jung et al.,
289 2021; Stinchcombe et al., 2023).

290 Material and Methods

291 **Constructs**

292 Receptors

293 Receptor sequences for SIRPβ1, Siglec 14, NKp44 and TREM-1 were inserted into the pHR-SIN-BX-Strep-
294 tag II plasmid as described by (Denham *et al.*, 2019). The same constructs containing the DAP12 adaptor
295 protein was also used.

296 Ligand anchors

297 For the ligand anchors DNA encoding the Igk leader sequence (bold), HA tag (italics), SpyTag
298 (underlined) bracketed by GGS linkers, and the hinge, transmembrane and intracellular regions of
299 mouse CD80, mouse CD43, or human CD52 (italics underlined) was inserted into the vector pEE14. To
300 express the long ligand anchor DNA encoding human CD4 (italics bold) was inserted between the SpyTag
301 and CD80 hinge. This included an R to D point mutation (underlined) to prevent CD4 binding MHC class
302 II. After expression CD52 anchor is cleaved and linked to GPI anchor at the serine residue marked in bold

303 CD80 anchor (short):

304 **M E T D T L L L W V L L L W V P G S T G D** *Y P Y D V P D Y A* T G G S A H I V M V D A Y K P T K G G S G G S *H*
305 *V S E D F T W E K P P E D P P D S K N T L V L F G A G F G A V I T V V V I V V I I K C F C K H R S C F R R N E A S*
306 *R E T N N S L T F G P E E A L A E Q T V F L*

CD80 anchor (long):

M E T D T L L L W V L L L W V P G S T G D *Y P Y D V P D Y A* T G G S A H I V M V D A Y K P T K G G S G G S ***K V V L G K K G D T V E L T C T A S Q K K S I Q F H W K N S N Q I K I L G N Q G S F L T K G P S K L N D D A D S R R S L W D Q G N F P L I I K N L K I E D S D T Y I C E V E D Q K E E V Q L L V F G L T A N S D T H L L Q G Q S L T L T L E S P P G S S P S V Q C R S P R G K N I Q G G K T L S V S Q L E L Q D S G T W T C T V L Q N Q K K V E F K I D I V V L A F Q K A S S I V Y K K E G E Q V E F S F P L A F T V E K L T G S G E L W W Q A E R A S S S K S W I T F D L K N K E V S V K R V T Q D P K L Q M G K K L P L H L T L P Q A L P Q Y A G S G N L T L A L E A K T G K L H Q E V N L V V M R A T Q L Q K N L T C E V W G P T S P K L M L S L K L E N K E A K V S K R E K A V W V L N P E A G M W Q C L L S D S G Q V L L E S N I K V L P T R S*** *H V S E D F T W E K P P E D P P D S K N T L V L F G A G F G A V I T V V V I V V I I K C F C K H R S C F R R N E A S R E T N N S L T F G P E E A L A E Q T V F L*

CD43 anchor:

M E T D T L L L W V L L L W V P G S T G D *Y P Y D V P D Y A T G G S* A H I V M V D A Y K P T K G G S G G S *Q E S S G M L L V P M L I A L V V V L A L V A L L L L W R Q R Q K R R T G A L T L S G G G K R N G V V D A W A G P A R V P D E E A T T T S G A G G N K G S E V L E T E G S G Q R P T L T T F F S R R K S R Q G S L V L E E L K P G S G P N L K G E E E P L V G S E D E A V E T P T S D G P Q A K D E A A P Q S L*

CD52 anchor:

M E T D T L L L W V L L L W V P G S T G D *Y P Y D V P D Y A T* G G S A H I V M V D A Y K P T K G G S G G S *S D T S Q T S S P* ***S*** *A S S N I S G G I F L F F V A N A I I H L F C F S*

Soluble proteins

Strep-Tactin-SpyCatcher sequence:

Strep-Tactin is underlined, SpyCatcher is in italics and the polyaspartate sequence is in bold.

M A E A G I T G T W Y N Q L G S T F I V T A G A D G A L T G T Y V T A R G N A E S R Y V L T G R Y D S A P A T D G S G T A L G W T V A W K N N Y R N A H S A T T W S G Q Y V G G A E A R I N T Q W L L T S G T T E A N A W K S T L V G H D T F T K V K P S A A S **D D D G D D D G D D D D** *S A T H I K F S K R D E D G K E L A G A T M E L R D S S G K T I S T W I S D G Q V K D F Y L Y P G K Y T F V E T A A P D G Y E V A T A I T F T V N E Q G Q V T V N G K A T K G D A H I*

Strep-Tactin sequence:

336 M A E A G I T G T W Y N Q L G S T F I V T A G A D G A L T G T Y V T A R G N A E S R Y V L T G R Y D S A P A T
337 D G S G T A L G W T V A W K N N Y R N A H S A T T W S G Q Y V G G A E A R I N T Q W L L T S G T T E A N A
338 W K S T L V G H D T F T K V K P S A A S

339 Dead Streptavidin sequence:

340 Bold amino acids mark substitutions in order to prevent binding to Strep tag II or biotin.

341 M A E A G I T G T W Y **A** Q L G **D** T F I V T A G A D G A L T G T Y E **A** A V G A E S R Y V L T G R Y D S A P A T D
342 G S G T A L G W T V A W K N N Y R N A H S A T T W S G Q Y V G G A E A R I N T Q W L L T S G T T E A N A W
343 K S T L V G H D T F T K V K P S A A S

344 GFP-SpyCatcher

345 The GFP-SpyCatcher construct was described in (Denham *et al.*, 2019).

346 **THP-1 cell lines**

347 THP-1 cells were maintained in RPMI-1640 media (Sigma-Aldrich #R8758) supplemented with 10% foetal
348 bovine serum (FBS) and 1 in 100 penicillin/streptomycin (Thermo Fisher Scientific #15140122) at 37 °C in
349 a 5% CO2 containing incubator.

350 **CHO cell lines**

351 Chinese Hamster Ovary (CHO) mock cells were maintained in DMEM (Sigma-Aldrich #D6429)
352 supplemented with 5% FBS and 1 in 100 penicillin/streptomycin. CHO ligand anchor cells (short and
353 long) were maintained in L-Glutamine-free DMEM (Sigma-Aldrich #D6546) supplemented with 10%
354 dialysed FBS (dialysed three times against 10 L PBS), 1 in 100 penicillin/streptomycin, 1x GSEM
355 supplement (Sigma-Aldrich #G9785) and 50 µM L-Methionine sulfoximine (Sigma-Aldrich #M5379).

356 **Lentiviral transduction of THP-1 cells**

357 Either receptor-expressing lentivector alone, or with the DAP12 adaptor-expressing lentivector, was co-
358 transfected with the lentiviral packaging plasmids pRSV-Rev (Addgene plasmd #12253), pMDLg/pRRE
359 (Addgene plasmd #12251) and pMD2.g (Addgene plasmd #12259) into HEK293T cells using X-
360 tremeGENETM HP (Sigma-Aldrich 6366546001) as per the manufacturer's instructions. Two days after
361 transfection, viral supernatants were harvested, filtered (0.45 µM syringe filter) and used for the
362 transduction of THP-1 cells in the presence of 5 µg mL^{-1} Polybrene.

363 **Analysing receptor and adaptor expression using flow cytometry and cell sorting by Fluorescence-**
364 **Activated Cell Sorting (FACS)**

365 Cells were analysed for receptor surface expression by flow cytometry using anti-Strep-tag II antibody
366 Oyster 645 (IBA Lifesciences #2-1555-050), or anti-Strep-tag II antibody (IBA Lifesciences #2-1507-001)
367 and anti-mouse IgG1 antibody Alexa Fluor 647 (Thermo Fisher Scientific #A-21240), on a Cytek DxP8.
368 Introduced adaptor expression was tested via expression of EmGFP encoded on the adaptor lentivector.
369 Cells were sorted for matched high expression of receptor plus introduced adaptor by fluorescence-
370 activated cell sorting (FACS) (MoFlo Astrios, Beckman Coulter).

371 **Transfection of CHO cells with various ligand anchors**

372 CHO cells were transfected with either pEE14 (CHO mock) or pEE14-ligand anchor (CHO ligand anchor)
373 using Xtreme-GENE 9^{TM} as per the manufacturer's instructions. Transfected lines were cultured in the
374 appropriate selection media after 48 hours.

375 **Checking ligand anchor expression by flow cytometry**

376 CHO Cells were analysed for ligand anchor surface expression by flow cytometry using anti-HA-Tag
377 antibody Alexa Fluor 647 (6E2; Cell Signalling Technology). Alternatively, cells were coupled with
378 saturating concentration of monovalent StrepTactin SpyCatcher. Biotin ATTO 647 was then added at 2
379 µM for 30 minutes. The cells were washed 3 times in PBS 1%BSA before they were fixed in PBS 1%
380 formaldehyde and analysed via flow cytometry.

381 **Expression and purification of monovalent and tetravalent Strep-Tactin-SpyCatcher**

382 Strep-Tactin SpyCatcher and dead streptavidin (monovalent) or Strep-Tactin SpyCatcher and Strep-
383 Tactin (tetravalent) expressed in Escherichia coli BL21-CodonPlus (DE3)-RIPL cells (Agilent Technologies
384 #230280) were combined and refolded from inclusion bodies. Inclusion bodies were washed in
385 BugBuster (Merck Millipore #70921) supplemented with lysozyme, protease inhibitors, DNase I and
386 magnesium sulphate as per the manufacturers' instructions. Subunits were then mixed at a 3:1 molar
387 ratio to improve the yield of the desired tetramer. The subunits were refolded by rapid dilution in cold
388 PBS and contaminates removed via precipitation using ammonium sulphate before additional
389 ammonium sulphate was added to precipitate the desired tetramer. Precipitated protein was
390 resuspended in 20 mM Tris pH 8.0, filtered (0.22 µm syringe filter), and loaded onto a Mono Q HR 5/5
391 column (GE Healthcare Life Sciences). Desired tetramers were eluted using a linear gradient of 0-0.5 M
392 NaCl in 20 mM Tris pH 8.0, concentrated, and buffer exchanged into 20 mM MES, 140 mM NaCl pH 6.0
393 (Denham *et al.*, 2019).

394 **Coupling CHO generic ligand cells**

395 Ligand anchor expressing or mock transduced CHO cells were incubated with various concentrations of
396 monovalent or tetravalent Strep-Tactin SpyCatcher in 20 mM MES, 140 mM NaCl, pH 6.0 and 1% BSA for
397 10 minutes at RT. Unbound Strep-Tactin SpyCatcher was removed by washing three times with PBS 1%
398 BSA.

399 **FACS Sorting of ligand anchor expressing CHO cells**

400 CHO short and long cells were coupled with a saturating concentration of monovalent Strep-Tactin
401 SpyCatcher. Biotin ATTO 647 (ATTO-TEC #AD 647-71) was then added at 2 µM for one hour and the
402 excess washed off with PBS 1 % BSA. The short and long CHO cells were then sorted for matched
403 expression of atto 647 signal corresponding to the expression level of ligand anchor using FACS (MoFlo
404 Astrios, Beckman Coulter).

405 **Biotin-4-fluorescein quenching assay**

406 The valency of purified monovalent and tetravalent Strep-Tactin SpyCatcher was measured using biotin-
407 4-fluorescein (Sigma-Aldrich #B9431-5MG) which when bound to Strep-Tactin become quenched.
408 Monovalent and tetravalent Strep-Tactin SpyCatcher was incubated with a titration of biotin-4-
409 fluorescein in black, opaque plates for 30 minutes at RT in PBS 1% BSA. Fluorescence was measured (λ_{ex}
410 485 nm, λ_{ex} 520 nm) using a plate reader. Fluorescence values were corrected for background
411 fluorescence before analysis. Negative control (buffer alone) data were fitted with the linear regression.
412 Sample data was fitted with a segmental linear regression, equation below, where X is the biotin-4-
413 fluorescein concentration, Y is fluorescence (AU), X0 is the biotin-4-fluorescein concentration at which
414 the line segments intersect. Slope1 was constrained to zero and is the gradient of the first line segment,
415 slope2 is the gradient of the second line segment. Intercept1 was constrained to zero and is the Y value
416 at which the first line segment intersects the Y axis. Slope2 was constrained to the gradient given by the
417 linear regression of the negative control.

418 $$Y1 = Intercept\ 1 + Slope1 * X$$

419 $$Y\ at\ X0 = Slope1 * X0 + Intercept1$$

420 $$Y2 = Y\ at\ X0 + Slope2 * (X - X0)$$

421 $$Y = IF\ (X < X0, Y1, Y2)$$

422 The X0 value was converted into an estimate of the number of biotin-binding sites per tetramer using
423 the concentration of Strep-Tactin SpyCatcher added and assuming complete binding of biotin-4-
424 fluorescein.

425 **Measurement of ligand binding sites on cells**

426 Ligand-anchor expressing or mock transduced CHO cells (3 x 10^6) were pre-incubated with a saturating
427 concentration of monovalent or tetravalent Strep-Tactin SpyCatcher. The above biotin-4-fluorescein
428 quenching assay was performed in the same manner but with a known number of cells. The X0 term
429 (calculated from the curve fit using equations above) was converted to the average number of binding
430 sites per cell using the equation below, where N is the average number of ligands per cell, X0 is the
431 saturation concentration of biotin-4-fluorescein extracted (M), V is the sample volume (L), N_A is
432 Avogadro's constant and C is the number of cells in the sample.

433 $$N = \frac{X0 * V * N_A}{C}$$

434 To measure relative levels of coupled SpyCatcher per cell, ligand cells were pre-incubated with a range
435 of concentrations of monovalent or tetravalent Strep-Tactin SpyCatcher or buffer alone (as a negative
436 control) before being incubated with 2 µM biotin ATTO 488 (ATTO-TEC #AD 488-71) pre-mixed with 40
437 µM biotin for 30 minutes at RT. The presence of biotin minimises the self-quenching activity of ATTO dye
438 observed with tetravalent Strep-Tactin. Cells were analysed by flow cytometry and the gMFI when cells
439 were incubated with buffer alone instead of Strep-Tactin SpyCatcher was subtracted from all
440 corresponding sample gMFI values. These values were then fitted with the single site binding model,
441 equation below, where Y is the gMFI (AU), Bmax is the maximum specific SpyCatcher binding indicated
442 by gMFI in AU, X is the [Streptactin-SpyCatcher] added (M) and K_D is the [SpyCatcher] that yields 50%
443 maximal binding to CHO cells (M).

444 $$Y = \frac{Bmax * X}{Kd + X}$$

445 To convert Y values into the average number of binding sites per ligand cell, the number of binding sites
446 per cell at saturating monovalent/tetravalent Strep-Tactin SpyCatcher concentration calculated in the
447 biotin-4-fluorescein assay was substituted into the equation above as Bmax. Y values were then re-
448 calculated following this adjustment. This method was followed in each independent experiment and
449 then an average value for the K_D and Bmax was used when combining replicates.

450 **Fluorescent recovery after photobleaching**

451 CHO cells (1 x10^5) expressing the three ligand anchors (CD80, CD43 and CD52) were transferred to a 35
452 mm glass bottom dish one day before imaging. To prepare cells for imaging each dish was washed 3
453 times with coupling buffer plus 10 % FBS. SpyCatcher-GFP was then added in excess (approximately 10
454 µM) and left for 10 minutes. Before washing the cells three times in PBS 1 % BSA 10 % FBS. Cells were
455 transferred to the Olympus FV1200 laser scanning microscope with 37 °C chamber for equilibration. The

456 60X magnification lens was used to locate cells spread over the glass coverslip. A small area of the cell
457 (approximately 10 %) was selected a few control images were taken before a 20 second bleach
458 performed. A time lapse series of images was then taken to track the recovery of the GFP signal.

459 Time lapse image series were imported into ImageJ for analysis. For each time lapse the bleach area was
460 selected (bleach) along with a control area which was taken to be the rest of the cell contact with the
461 glass (control area) and a negative control area around the outside of the cell (negative). Firstly, the
462 intensity from the negative area was subtracted from the bleach and control area. The bleach area was
463 then divided by the control area for each time frame and these values were normalised to the control
464 image before the bleach was performed. These values were then plotted against time and the equation
465 below used to find the half time for each ligand anchor.

466 $$Y = Y0 + (Plateau - Y0) * (1 - e^{-K*x})$$

467 Where Y0 is the value when X (time) is zero, Plateau is the Y value at infinite times and K is the rate
468 constant from which the half time is derived.

469 The half time value could then be converted into the diffusion coefficient using the equation below
470 (Soumpasis, 1983).

471 $$Diffusion\ coefficient = 0.224 * r^2 / half\ time$$

472 Where 0.224 is a constant for a circular bleach area, r is the radius of the bleach area, and the half time
473 is the derived from fitting the one phase association equation to the bleach recovery above.

474 **Ligand turnover**

475 CHO ligand anchor cells were incubated with 15 µM monovalent Strep-Tactin SpyCatcher (or buffer
476 alone) as described above and incubated at 37 °C to match stimulation assays for the time points
477 indicated. Cells were analysed for generic ligand surface expression using ATTO 488 biotin as above and
478 normalised to the geometric fluorescence intensity value at time 0. To calculate the decay, the gMFI
479 values were fitted with the equation below where Y0 is the Y value when X = 0, Plateau is the Y value at
480 which the curve reaches a plateau, X is time in minutes, and K is the rate constant in inverse minutes.

481 $$Y = (\mathrm{Y0} - \mathrm{Plateau}).e^{-K.X} + \mathrm{Plateau}$$

482 **IL-8 production**

483 CHO ligand anchor cells (2 x 10^5) coupled with either monovalent/tetravalent Strep-Tactin SpyCatcher or
484 buffer alone were mixed with single Strep-tag II tagged receptor and adaptor expressing THP-1 or
485 untransduced THP-1 cells (1 x 10^5) in DMEM 5% FBS, 1 in 100 penicillin/streptomycin, 2 µg mL^{-1} avidin.

486 Cells were incubated in a 37 °C 10% CO2 containing incubator for 20 hours. Supernatants were
487 harvested and assayed for IL-8 by ELISA following manufacturer's instructions (Thermo Fisher Scientific
488 #88808688).

489 **Conjugation assays**

490 Ligand cells were stained with CellTrace Far Red (Thermo Fisher Scientific #C34564) at a final
491 concentration of 1 µM in PBS at a density of 1 x 10^6 cells per ml. THP-1 receptor cells were stained with
492 CellTrace Violet (Thermo Fisher Scientific #C34557) at a final concentration of 1 µM in PBS for 20
493 minutes. CHO Ligand cells (4 x 10^5) coupled with either monovalent/tetravalent Strep-Tactin SpyCatcher
494 were mixed with (2 x 10^5) THP-1 cells in PBS 1 % BSA on Ice for 1 hour. Conjugation efficacy was
495 analysed by flow cytometry.

496 Due to experimental constraints stimulation and conjugation assays were completed on successive days.
497 However, we confirmed that the same result was observed when the stimulation and conjugation assays
498 were performed in parallel on the same day by splitting the cells in half for each assay (Supplementary
499 Figure 2)

500 **Data analysis**

501 For receptor stimulation assays, IL-8 concentrations in negative controls (where CHO cells were pre-
502 incubated with buffer alone instead of Strep-Tactin SpyCatcher) were subtracted from corresponding
503 sample IL-8 concentrations to correct for background levels. Dose-response curves were then fitted with
504 the below equation where Y is the measured cell response (pg mL^{-1}), Bottom and Top are the minimum
505 and maximum cell response respectively (pg mL^{-1}), EC50 is the number of binding sites per cell that
506 yields a half maximal response, X is the number of binding sites per cell and Hill slope relates to the
507 steepness of the curve.

508 $$Y = Bottom + \frac{(X^{Hillslope})(Top - Bottom)}{(X^{Hillslope} + EC50^{Hillslope})}$$

509 For conjugate assays the percentage of THP-1 cells forming conjugates was calculated using the formula
510 below. The data was then fit using the same dose response equation above except with X being the
511 percentage of THP-1 cells in conjugates, normalized where indicated.

512 $$Receptor\ cells\ in\ Conjugates\ (\%) = \frac{Double\ positive\ events}{Receptor\ only\ events + Double\ positive\ events} * 100$$

513 To plot stimulation as a function of conjugation the average number of binding sites used in the
514 stimulation assay were interpolated from the fit of the conjugation data using the four parameter dose

515 response model. The IL-8 values from the stimulation were then plotted against the interpolated values
516 of conjugate formation.

517 For statistical analysis F tests, t tests ANOVA were performed as appropriate and results presented with
518 the following symbols: ns, not significant ; * , $p < 0.05$; **, $p < 0.01$; ***, $p < 0.001$; ****, $p < 0.0001$.

519 Acknowledgements

520 We acknowledge Mark Howarth for providing Strep-Tactin, streptavidin, SpyTag and SpyCatcher
521 constructs and for helpful discussions and advice. We thank Marion H Brown and Omer Dushek and
522 their groups for helpful discussion.
523 This work was supported by a Wellcome Trust Senior Investigator Award (P.A.v.d.M., grant reference:
524 101799/Z/13/Z) and a Nuffield Medical Fellowship from the Australian Academy of Science (J.G., grant
525 reference: #1016848).
526

527 Author Contributions

528 The study was conceived by PAvdM and JG, the experiments were performed by MIB with reagents
529 prepared by RLP and EMD, the paper was drafted by MIB and PAvdM and finalized by all authors.

530 Competing interests

531 PAvdM is a founder of MatchBio Limited.

532 ## References

533

534 Al-Aghbar MA, Chu Y-S, Chen B-M, Roffler SR. 2018. High-Affinity Ligands Can Trigger T Cell Receptor
535 Signaling Without CD45 Segregation. *Frontiers in immunology* **9**:523. doi:10.3389/fimmu.2018.00713

536 Angata T, Hayakawa T, Yamanaka M, Varki A, Nakamura M. 2006. Discovery of Siglec-14, a novel sialic
537 acid receptor undergoing concerted evolution with Siglec-5 in primates. *FASEB J* **20**:1964–1973.
538 doi:10.1096/fj.06-5800com

539 Bakalar MH, Joffe AM, Schmid EM, Son S, Podolski M, Fletcher DA. 2018. Size-Dependent Segregation
540 Controls Macrophage Phagocytosis of Antibody-Opsonized Targets. *Cell* **174**:131–142.
541 doi:10.1016/j.cell.2018.05.059

542 Barclay AN, Brown MH, Law SKA, McKnight AJ, Tomlinson MG, van der Merwe PA. 1997. The Leucocyte
543 Antigen Factsbook, 2nd ed, Academic Press. Academic Press.

544 Boniface JJ, Boniface J, Rabinowitz JD, Rabinowitz J, Wulfing C, Hampl J, Reich Z, Altman J, Altman JD,
545 Kantor RM, Kantor R, Beeson C, McConnell HM, McConnell H, Davis M M, Davis Mark M. 1998.
546 Initiation of signal transduction through the T cell receptor requires the multivalent engagement of
547 peptide/MHC ligands [corrected]. *IMMUNITY* **9**:459–466.

548 Burroughs NJ, Lazic Z, van der Merwe PA. 2006. Ligand detection and discrimination by spatial
549 relocalization: A kinase-phosphatase segregation model of TCR activation. *Biophysical journal*
550 **91**:1619–1629. doi:10.1529/biophysj.105.080044

551 Chang VT, Fernandes RA, Ganzinger KA, Lee SF, Siebold C, McColl J, Jönsson P, Palayret M, Harlos K,
552 Coles CH, Jones EY, Lui Y, Huang E, Gilbert RJC, Klenerman D, Aricescu AR, Davis SJ. 2016. Initiation of
553 T cell signaling by CD45 segregation at "close contacts." *Nat Immunol* **17**:574–582.
554 doi:10.1038/ni.3392

555 Chen B-M, Al-Aghbar MA, Lee Chien-Hsin, Chang T-C, Su Y-C, Li Y-C, Chang S-E, Chen C-C, Chung T-H, Liao
556 Y-C, Lee Chau-Hwang, Roffler SR. 2017. The Affinity of Elongated Membrane-Tethered Ligands
557 Determines Potency of T Cell Receptor Triggering. *Front Immunol* **8**:793.
558 doi:10.3389/fimmu.2017.00793

559 Chen KY, Jenkins E, Körbel M, Ponjavic A, Lippert AH, Santos AM, Ashman N, O'Brien-Ball C, McBride J,
560 Klenerman D, Davis SJ. 2021. Trapping or slowing the diffusion of T cell receptors at close contacts
561 initiates T cell signaling. *Proc National Acad Sci* **118**:e2024250118. doi:10.1073/pnas.2024250118

562 Choudhuri K, Wiseman D, Brown MH, Gould K, van der Merwe PA. 2005. T-cell receptor triggering is
563 critically dependent on the dimensions of its peptide-MHC ligand. *Nature* **436**:578–582.
564 doi:10.1038/nature03843

565 Cochran JR, Cameron TO, Stern LJ. 2000. The Relationship of MHC-Peptide Binding and T Cell Activation
566 Probed Using Chemically Defined MHC Class II Oligomers. *Immunity* **12**:241–250. doi:10.1016/s1074-
567 7613(00)80177-6

568 Cordoba S-P, Choudhuri K, Zhang H, Bridge M, Basat AB, Dustin ML, van der Merwe PA. 2013. The large
569 ectodomains of CD45 and CD148 regulate their segregation from and inhibition of ligated T-cell
570 receptor. *Blood* **121**:4295–4302. doi:10.1182/blood-2012-07-442251

571 Cornish AL, Freeman S, Forbes G, Ni J, Zhang M, Cepeda M, Gentz R, Augustus M, Carter KC, Crocker PR.
572 1998. Characterization of Siglec-5, a Novel Glycoprotein Expressed on Myeloid Cells Related to CD33.
573 *Blood* **92**:2123–2132. doi:10.1182/blood.v92.6.2123.418k20_2123_2132

574 Crocker PR, Paulson JC, Varki A. 2007. Siglecs and their roles in the immune system. *Nature Reviews*
575 *Immunology* **7**:255–266. doi:10.1038/nri2056

576 Davis SJ, van der Merwe PA. 2006. The kinetic-segregation model: TCR triggering and beyond. *Nature*
577 *Immunology* **7**:803–809. doi:10.1038/ni1369

578 Davis SJ, van der Merwe PA. 1996. The structure and ligand interactions of CD2: implications for T-cell
579 function. *Immunol Today* **17**:177–187. doi:10.1016/0167-5699(96)80617-7

580 Denham EM, Barton MI, Black SM, Bridge MJ, Wet B de, Paterson RL, van der Merwe PA, Goyette J.
581 2019. A generic cell surface ligand system for studying cell–cell recognition. *Plos Biol* **17**:e3000549.
582 doi:10.1371/journal.pbio.3000549

583 Dushek O, Goyette J, van der Merwe PA. 2012. Non-catalytic tyrosine-phosphorylated receptors.
584 *Immunological Reviews* **250**:258–276. doi:10.1111/imr.12008

585 Ford JW, McVicar DW. 2009. TREM and TREM-like receptors in inflammation and disease. *Current*
586 *opinion in immunology* **21**:38–46. doi:10.1016/j.coi.2009.01.009

587 Göhring J, Kellner F, Schrangl L, Platzer R, Klotzsch E, Stockinger H, Huppa JB, Schütz GJ. 2021. Temporal
588 analysis of T-cell receptor-imposed forces via quantitative single molecule FRET measurements. *Nat*
589 *Commun* **12**:2502. doi:10.1038/s41467-021-22775-z

590 Goodridge HS, Reyes CN, Becker CA, Katsumoto TR, Ma J, Wolf AJ, Bose N, Chan ASH, Magee AS,
591 Danielson ME, Weiss A, Vasilakos JP, Underhill DM. 2011. Activation of the innate immune receptor
592 Dectin-1 upon formation of a 'phagocytic synapse.' *Nature* **472**:471–475. doi:10.1038/nature10071

593 Goyette J, Nieves DJ, Ma Y, Gaus K. 2019. How does T cell receptor clustering impact on signal
594 transduction? *Journal of cell science* **132**:jcs226423. doi:10.1242/jcs.226423

595 James JR, Vale RD. 2012. Biophysical mechanism of T-cell receptor triggering in a reconstituted system.
596 *Nature* **487**:64–69. doi:10.1038/nature11220

597 Jenkins E, Körbel M, O'Brien-Ball C, McColl J, Chen KY, Kotowski M, Humphrey J, Lippert AH, Brouwer H,
598 Santos AM, Lee SF, Davis SJ, Klenerman D. 2023. Antigen discrimination by T cells relies on size-
599 constrained microvillar contact. *Nat Commun* **14**:1611. doi:10.1038/s41467-023-36855-9

600 June CH, Sadelain M. 2018. Chimeric Antigen Receptor Therapy. *New Engl J Med* **379**:64–73.
601 doi:10.1056/nejmra1706169

602 Jung Y, Wen L, Altman A, Ley K. 2021. CD45 pre-exclusion from the tips of T cell microvilli prior to
603 antigen recognition. *Nat Commun* **12**:3872. doi:10.1038/s41467-021-23792-8

604 Köhler K, Xiong S, Brzostek J, Mehrabi M, Eissmann P, Harrison A, Cordoba S-P, Oddos S, Miloserdov V,
605 Gould K, Burroughs NJ, van der Merwe PA, Davis DM. 2010. Matched sizes of activating and
606 inhibitory receptor/ligand pairs are required for optimal signal integration by human natural killer
607 cells. *PLOS One* **5**:e15374. doi:10.1371/journal.pone.0015374

608 Labanieh L, Mackall CL. 2023. CAR immune cells: design principles, resistance and the next generation.
609 *Nature* **614**:635–648. doi:10.1038/s41586-023-05707-3

610 Lanier LL. 2008. DAP10- and DAP12-associated receptors in innate immunity. *Immunological reviews*
611 **227**:150–160. doi:10.1111/j.1600-065x.2008.00720.x

612 Li Y-C, Chen B-M, Wu P-C, Cheng T-L, Kao L-S, Tao M-H, Lieber A, Roffler SR. 2010. Cutting Edge:
613 Mechanical Forces Acting on T Cells Immobilized via the TCR Complex Can Trigger TCR Signaling. *J*
614 *Immunol* **184**:5959–5963. doi:10.4049/jimmunol.0900775

615 Lim H-S, Cordoba S-P, Dushek O, Goyette J, Taylor A, Rudd CE, van der Merwe PA. 2015. Costimulation
616 of IL-2 Production through CD28 Is Dependent on the Size of Its Ligand. *Journal of immunology*
617 *(Baltimore, Md : 1950)* **195**:5432–5439. doi:10.4049/jimmunol.1500707

618 Locksley RM, Killeen N, Lenardo MJ. 2001. The TNF and TNF Receptor Superfamilies Integrating
619 Mammalian Biology. *Cell* **104**:487–501. doi:10.1016/s0092-8674(01)00237-9

620 Ma Z, Janmey PA, Finkel TH. 2008. The receptor deformation model of TCR triggering. *The FASEB Journal*
621 **22**:1002–1008. doi:10.1096/fj.07-9331hyp

622 van der Merwe PA, Barclay AN. 1994. Transient intercellular adhesion: the importance of weak protein-
623 protein interactions. *Trends Biochem Sci* **19**:354–358. doi:10.1016/0968-0004(94)90109-0

624 van der Merwe PA, Davis SJ, Shaw AS, Dustin ML. 2000. Cytoskeletal polarization and redistribution of
625 cell-surface molecules during T cell antigen recognition. *Semin Immunol* **12**:5–21.
626 doi:10.1006/smim.2000.0203

627 Milstein O, Tseng S-Y, Starr T, Llodra J, Nans A, Liu M, Wild MK, van der Merwe PA, Stokes DL, Reisner Y,
628 Dustin ML. 2008. Nanoscale Increases in CD2-CD48-mediated Intermembrane Spacing Decrease
629 Adhesion and Reorganize the Immunological Synapse*. *J Biol Chem* **283**:34414–34422.
630 doi:10.1074/jbc.m804756200

631 O'Shea JJ, McVicar DW, Bailey TL, Burns C, Smyth MJ. 1992. Activation of human peripheral blood T
632 lymphocytes by pharmacological induction of protein-tyrosine phosphorylation. *Proceedings of the*
633 *National Academy of Sciences of the United States of America* **89**:10306–10310.

634 Parodi M, Favoreel H, Candiano G, Gaggero S, Sivori S, Mingari MC, Moretta L, Vitale M, Cantoni C. 2019.
635 NKp44-NKp44 Ligand Interactions in the Regulation of Natural Killer Cells and Other Innate Lymphoid
636 Cells in Humans. *Front Immunol* **10**:719. doi:10.3389/fimmu.2019.00719

637 Patel A, Andre V, Eguiguren SB, Barton MI, Denham EM, Pettmann J, Morch AM, Kutuzov M, Siller-Farfan
638 JA, Dustin ML, van der Merwe PA, Dushek O. 2023. Using CombiCells, a platform enabling titration
639 and combinatorial display of cell surface ligands, to investigate the sensitivity and costimulatory
640 requirements of TCRs and CARs. doi:10.1101/2023.06.15.545075

641 Razvag Y, Neve-Oz Y, Sajman J, Reches M, Sherman E. 2018. Nanoscale kinetic segregation of TCR and
642 CD45 in engaged microvilli facilitates early T cell activation. *Nature Communications* **9**:732.
643 doi:10.1038/s41467-018-03127-w

644 Sadelain M. 2016. Chimeric antigen receptors: driving immunology towards synthetic biology. *Current*
645 *opinion in immunology* **41**:68–76. doi:10.1016/j.coi.2016.06.004

646 Schamel WW, Alarcón B, Minguet S. 2019. The TCR is an allosterically regulated macromolecular
647 machinery changing its conformation while working. *Immunological reviews* **291**:8–25.
648 doi:10.1111/imr.12788

649 Schmid EM, Bakalar MH, Choudhuri K, Weichsel J, Ann HS, Geissler PL, Dustin ML, Fletcher DA. 2016.
650 Size-dependent protein segregation at membrane interfaces. *Nature Physics*. doi:10.1038/nphys3678

651 Secrist JP, Burns LA, Karnitz L, Koretzky GA, Abraham RT. 1993. Stimulatory effects of the protein
652 tyrosine phosphatase inhibitor, pervanadate, on T-cell activation events. *Journal of Biological*
653 *Chemistry* **268**:5886–5893.

654 Sharma P, Allison JP. 2015. The future of immune checkpoint therapy. *Science* **348**:56–61.
655 doi:10.1126/science.aaa8172

656 Shilts J, Severin Y, Galaway F, Müller-Sienerth N, Chong Z-S, Pritchard S, Teichmann S, Vento-Tormo R,
657 Snijder B, Wright GJ. 2022. A physical wiring diagram for the human immune system. *Nature*
658 **608**:397–404. doi:10.1038/s41586-022-05028-x

659 Springer TA. 1990. Adhesion receptors of the immune system. *Nature* **346**:425–434.
660 doi:10.1038/346425a0

661 Stinchcombe JC, Asano Y, Kaufman CJG, Böhlig K, Peddie CJ, Collinson LM, Nadler A, Griffiths GM. 2023.
662 Ectocytosis renders T cell receptor signaling self-limiting at the immune synapse. *Science* **380**:818–
663 823. doi:10.1126/science.abp8933

664 Ullrich A, Schlessinger J. 1990. Signal transduction by receptors with tyrosine kinase activity. *Cell*
665 **61**:203–212. doi:10.1016/0092-8674(90)90801-k

666 Varma R, Campi G, Yokosuka T, Saito T, Dustin ML. 2006. T Cell Receptor-Proximal Signals Are Sustained
667 in Peripheral Microclusters and Terminated in the Central Supramolecular Activation Cluster.
668 *Immunity* **25**:117–127. doi:10.1016/j.immuni.2006.04.010

669 Wild MK, Cambiaggi A, Brown MH, Davies EA, Ohno H, Saito T, van der Merwe PA. 1999. Dependence of
670 T Cell Antigen Recognition on the Dimensions of an Accessory Receptor–Ligand Complex. *J Exp*
671 *Medicine* **190**:31–42. doi:10.1084/jem.190.1.31

672 Wilhelm KB, Morita S, McAffee DB, Kim S, O'Dair MK, Groves JT. 2021. Height, but not binding epitope,
673 affects the potency of synthetic TCR agonists. *Biophys J* **120**:3869–3880.
674 doi:10.1016/j.bpj.2021.08.027

675 Wu H, Kwong PD, Hendrickson WA. 1997. Dimeric association and segmental variability in the structure
676 of human CD4. *Nature* **387**:527–530. doi:10.1038/387527a0

677 Xiao Q, Zhang X, Tu L, Cao J, Hinrichs CS, Su X. 2022. Size-dependent activation of CAR-T cells. *Sci*
678 *Immunol* **7**:eabl3995. doi:10.1126/sciimmunol.abl3995

679 Zhu C, Chen W, Lou J, Rittase W, Li K. 2019. Mechanosensing through immunoreceptors. *Nat Immunol*
680 **20**:1269–1278. doi:10.1038/s41590-019-0491-1

681

682 ## Figure legends

683 **Figure 1 Testing the effect of increasing ligand length on NTR activation**

684 (A) Schematic depiction of the components of the generic ligand system used to test the effect of
685 increasing ligand length and valency. The shared DAP-12 signalling homodimer is grey. With tetravalent
686 streptactin (not shown) all four of the binding sites are able to bind Steptag II (B) Representative flow
687 cytometry data from a conjugation assay between SIRPβ1 expressing THP1 receptor cells and CHO cells
688 expressing short ligands coupled with the indicated concentration of monovalent Strep-Tactin
689 SpyCatcher. Receptor and ligand cells were stained with CellTrace Violet and Far Red, respectively, and
690 events in the upper right quadrant were presumed to be conjugates. (C) Conjugation of (left panel) and
691 IL-8 secretion by (middle panel) SIRPβ1 expressing THP1 cells incubated with CHO cells expressing the
692 indicated number of short (blue) or long (red) monovalent ligands, measured as described in the
693 Materials and Methods using parameters determined in sFigure 1. IL-8 secretion is plotted against
694 conjugation in the right panel. These are representative results from three independent experiments,
695 which are combined in Figure 2A for statistical analysis. Due to experimental constraints the stimulation
696 and conjugation assays in this (and subsequent) experiment(s) were performed on successive days. The
697 same result was obtained when performed on the same day (sFigure 2).

698 **Figure 2: The effect of NTR ligand length on activation via four NTRs.**

699 THP-1 cells expressing (A) SIRPβ1, (B) Siglec 14, (C) NKp44 or (D) TREM-1 with N-terminal StrepTagII
700 peptides were incubated with CHO cells expressing the indicated numbers of short (blue) or long (red)
701 monovalent generic ligand binding sites and conjugate formation (left panel) and IL-8 release (middle
702 panel) measured. Ligand binding sites were determined as described in the Materials and Methods
703 using parameters determined in sFigure 1. The IL-8 release versus conjugation level is plotted in the
704 right panels. The data from three biological replicates (including one SIRPβ1 replicate shown in Figure 1)
705 are plotted with the data normalised to the level of conjugation or stimulation achieved with the short
706 ligand within each replicate. The data were fitted as described in the Materials and Methods and an F
707 test was used to test the significance of differences between the fits.

708 **Figure 3: Effect of ligand anchor on SIRPβ1 stimulation**

709 (A) Schematic depiction of the components of the generic ligand system used to test the effect of
710 varying the ligand anchor. (B) The diffusion coefficients of the different ligand anchors were measured
711 by FRAP after coupling GFP-Spycatcher. The mean and SD from three independent experiments were
712 compared by ANOVA. (C) THP-1 cells expressing SIRPβ1 with an N-terminal StrepTagII peptide were
713 incubated with CHO cells expressing the indicated number of ligand binding sites with CD80 (blue), CD43

714 (orange) or CD52 (green) anchors, and conjugate formation (left panel) and IL-8 release (right panel)
715 measured. Ligand binding sites were determined as described in the Materials and Methods using
716 parameters determined in sFigure 4. The IL-8 release versus conjugation level is plotted in the right
717 panel. The data from three biological replicates are plotted with the data normalised to the level of
718 conjugation or stimulation achieved with the CD52 ligand anchor within each replicate. These data were
719 fitted as described in the Materials and Methods and an F test was used to test the significance of
720 differences between the fits collectively and pairwise (Tables).

721 **Figure 4: Effect of ligand valency on NTR stimulation.**

722 THP-1 cells expressing (A) SIRPβ1, (B) Siglec 14, (C) NKp44 or (D) TREM-1 with N-terminal StrepTagII
723 peptides were incubated with CHO cells expressing the indicated numbers of monovalent (filled circles)
724 or tetravalent (open circles) short generic ligand binding sites and conjugate formation (left panel) and
725 IL-8 release (middle panel) measured. Ligand binding sites were determined as described in the
726 Materials and Methods using parameters determined in sFigure 6. The IL-8 release versus conjugation
727 level is plotted in the right panels. The data from three biological replicates are plotted with the data
728 normalised to the level of conjugation or stimulation achieved with the short tetravalent ligand within
729 each replicate. These data were fitted as described in the Materials and Methods and an F test was used
730 to test the significance of differences between the fits.

731 **Figure 5: The effect of NTR ligand length on activation by tetravalent ligands**

732 THP-1 cells expressing (A) SIRPβ1, (B) Siglec 14, (C) NKp44 or (D) TREM-1 with N-terminal StrepTagII
733 peptides were incubated with CHO cells expressing the indicated numbers of short (blue) or long (red)
734 tetravalent ligand binding sites and conjugate formation (left panel) and IL-8 release (middle panel)
735 measured. Ligand binding sites were determined as described in the Materials and Methods using
736 parameters determined in sFigure 9. The IL-8 release versus conjugation level is plotted in the right
737 panels. The data from three biological replicates are plotted with the data normalised to the level of
738 conjugation or stimulation achieved with the short tetravalent ligand within each replicate. These data
739 were fitted as described in the Materials and Methods and an F test was used to test the significance of
740 differences between the fits.

741

742 ## Supplementay Figure legends

743 **sFigure 1. Measuring the K_D and maximum number of binding sites on CHO cell expressing short and**
744 **long CD80 ligand anchors**

745 (A) Short (blue) or long (red) CD80 ligand CHO cells were incubated with the indicated concentration of
746 monovalent StrepTactin SpyCatcher before labelling with biotin Atto 488 followed by flow cytometry. A
747 one site simple binding model was fitted to the data (lines) to determine the K_D. (B) The mean and SD of
748 K_D values from six independent experiments were compared using a t test. (C) Short or long CD80 ligand
749 CHO cells or control (empty, grey) CHO cells were incubated with a saturating concentration (15 μM) of
750 monovalent StrepTactin SpyCatcher before mixing with the indicated concentration of biotin-4-
751 fluorescein and the unquenched fluorescence in the media measured after binding. (D) The mean and
752 SD of the maximum number of binding sites per cell from six independent experiments were compared
753 using a t test.

754 **sFigure 2. Testing the effect of increasing ligand length on NTR activation**

755 Repeat of experiment Figure 1 with both conjugation and stimulation assays performed on the same day
756 with the same cells split. THP-1 cells expressing SIRPβ1 were incubated with CHO cells expressing the
757 indicated numbers of short (blue) or long (red) generic ligand binding sites and conjugate formation (A)
758 and IL-8 release (B) measured. Ligand binding sites were determined as described in the Materials and
759 Methods using parameters determined in sFigure 1. The IL-8 release versus conjugation level is plotted
760 in (C).

761 **sFigure 3. The effect of NTR length on activation.**

762 The data from Figure 2 has been reanalysed to enable comparison between NTRs. THP-1 cells expressing
763 the indicated NTR with N-terminal StrepTagII peptides were incubated with CHO cells expressing the
764 indicated numbers of short (A) or long (B) generic ligand binding sites and conjugate formation (left
765 panel) and IL-8 release (middle panel) measured. The IL-8 release versus conjugation level is plotted in
766 the right panels. The data were fitted as described in the Materials and Methods and an F test was used
767 to test the significance of differences between the fits collectively (panels) and pairwise (corresponding
768 Tables).

769 **sFigure 4. K_D and maximum generic binding sites on CHO cell expressing different ligand anchors**

770 (A) Mean and SD of K_D values determined as in sFigure 1 from nine independent experiments (B) Mean
771 and SD of maximum number of binding sites determined as in sFigures 1 from six independent
772 experiments. To enable comparison to monovalent sites the tetravalent values divided by four, labelled
773 (/4), were also plotted.

774 **sFigure 5. Turnover of ligand anchor at the cell surface.**

775 (A-C) Monovalent StrepTactin SpyCatcher was coupled to CHO cells expressing the indicated ligand
776 anchor and cells incubated at 37 C for the indicated times. Cells were stained with biotin ATTO 488 and
777 analysed by flow cytometry to assess the level of the cell surface StrepTactin. The graphs show the
778 relative level of ligand expression with the maximum normalised to time zero. The data is a
779 representative of three biological replicates and was fit with an exponential one phase decay model. (D)
780 The mean and SD of the half-time for loss from the cell surface for three biological replicates were
781 compared by ANOVA.

782 **sFigure 6. Measuring the K_D and maximum number of binding sites on CHO cell presenting**
783 **monovalent or tetravalent StrepTactin SpyCatcher**

784 (A) Short CD80 ligand CHO cells were incubated with the indicated concentration of monovalent (closed
785 circles) or tetravalent (open circles) StrepTactin SpyCatcher before labelling with biotin Atto 488
786 followed by flow cytometry. A one site simple binding model was fitted to the data (lines) to determine
787 the K_D. (B) The mean and SD of K_D values from eight independent experiments were compared using a t
788 test. (C) Short CD80 ligand CHO cells or control (empty, grey) CHO cells were incubated with a saturating
789 concentration monovalent (10 μM) or tetravalent (10 μM) StrepTactin SpyCatcher before mixing with
790 the indicated concentration of biotin-4-fluorescein and the unquenched florescence in the media
791 measured after binding. (D) The mean and SD of the maximum number of binding sites per cell from five
792 independent experiments were compared by ANOVA. To enable comparison to monovalent sites the
793 tetravalent values divided by four were also plotted.

794 **sFigure 7. Effect of anchor on NTR stimulation by multivalent ligand**

795 THP-1 cells expressing (A) SIRPβ1, (B) Siglec 14, (C) NKp44 or (D) TREM-1 with an N-terminal StrepTagII
796 peptide were incubated with CHO cells expressing the indicated number of monovalent (closed circles)
797 or multivalent (open circles) ligand binding sites with the indicated ligand anchors and IL-8 release
798 measured. Ligand binding sites were determined as described in the Materials and Methods using
799 parameters determined in sFigure 4. The data from three biological replicates are plotted with the data
800 normalised to the level of stimulation achieved with the CD80 ligand coupled with tetravalent ligand
801 within each replicate. These data were fitted as described in the Material and Methods and an F test
802 was used to test the significance of differences between the fits collectively and pairwise (Tables).

803 **sFigure 8. Effect of anchor on SIRPβ1 stimulation by multivalent ligand**

804 THP-1 cells expressing SIRPβ1 with an N-terminal StrepTagII peptide were incubated with CHO cells
805 expressing the indicated number of ligand binding sites presented on monovalent (closed circles) or

806 multivalent (open circles) ligand and conjugate formation (left panel) and IL-8 release (middle panel)
807 were measured. Ligand binding sites were determined as described in the Materials and Methods using
808 parameters determined in sFigure 4. The IL-8 release versus conjugation level is plotted in the right
809 panel. The data from three biological replicates are plotted with the data normalised to the level of
810 conjugation or stimulation achieved with the tetravalent ligand within each replicate. These data were
811 fitted as described in the Material and Methods and an F test was used to test the significance of
812 differences between the fits.

813 **sFigure 9. Measuring the K_D and maximum number of binding sites on CHO cell presenting tetravalent**
814 **StrepTactin SpyCatcher coupled to short versus long ligand anchors**

815 (A) Short (blue) or long (red) CD80 ligand CHO cells were incubated with the indicated concentration of
816 tetravalent StrepTactin SpyCatcher before labelling with biotin Atto 488 followed by flow cytometry. A
817 one site simple binding model was fitted to the data (lines) to determine the K_D. (B) The mean and SD of
818 K_D values from six independent experiments were compared using a t test. (C) Short or long CD80 ligand
819 CHO cells or control (empty, grey) CHO cells were incubated with a saturating concentration (10 μM) of
820 tetravalent StrepTactin SpyCatcher before mixing with the indicated concentration of biotin-4-
821 fluorescein and the unquenched florescence in the media measured after binding. (D) The mean and SD
822 of the maximum number of binding sites per cell from six independent experiments were compared
823 using a t test.

824

Figure 1

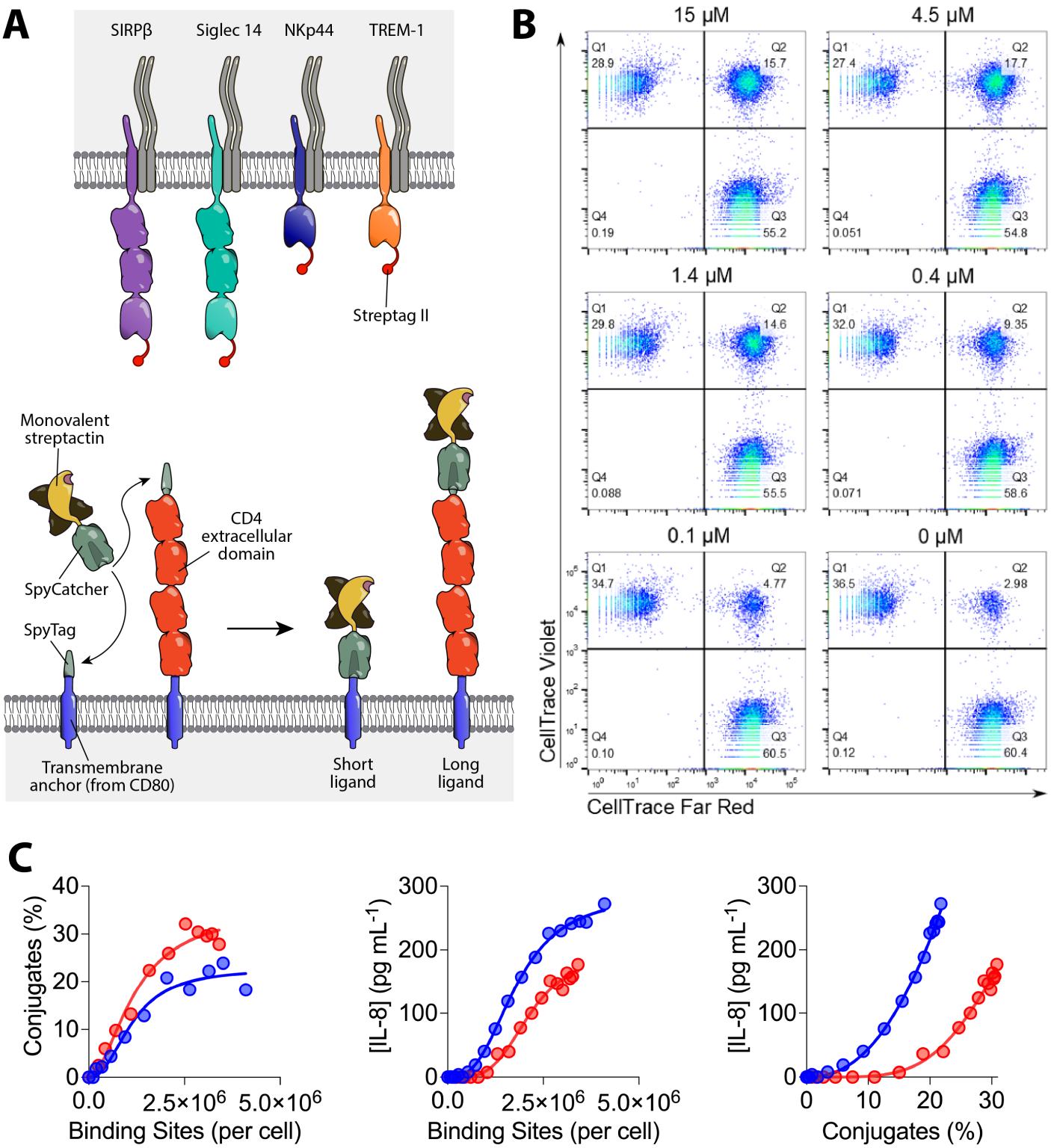
A
SIRPβ
Siglec 14
NKp44
TREM-1
Streptag II
Monovalent streptactin
SpyCatcher
SpyTag
CD4 extracellular domain
Transmembrane anchor (from CD80)
Short ligand
Long ligand
B
15 μM
4.5 μM
1.4 μM
0.4 μM
0.1 μM
0 μM
CellTrace Violet
CellTrace Far Red
C
Conjugates (%)
Binding Sites (per cell)
[IL-8] (pg mL-1)
Conjugates (%)

Figure 2

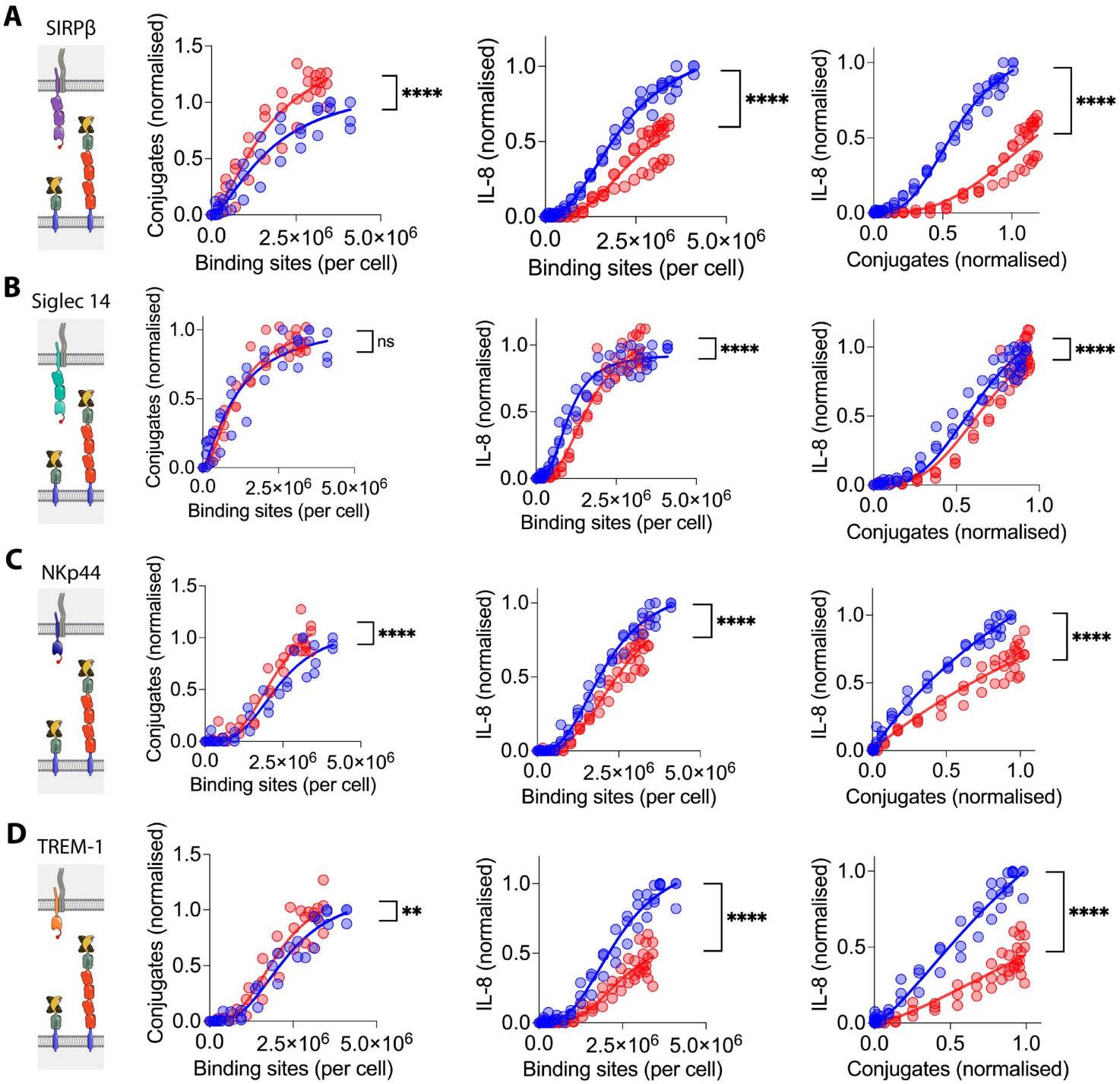
A
SIRPβ
Conjugates (normalised)
Binding sites (per cell)
IL-8 (normalised)
Conjugates (normalised)
****
B
Siglec 14
ns
C
NKp44
D
TREM-1
**

Figure 3

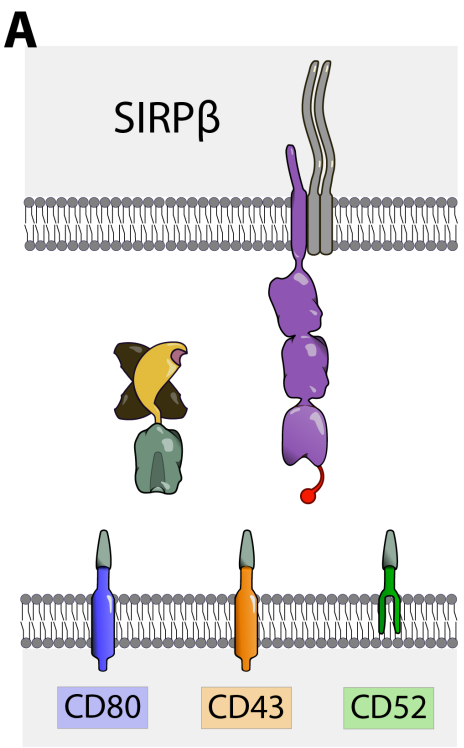

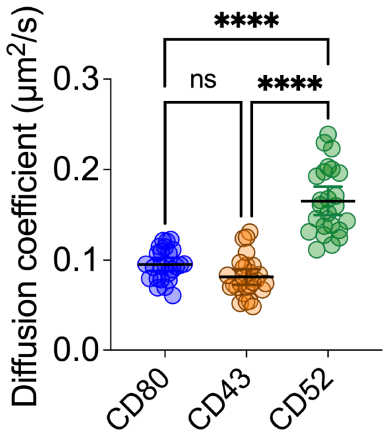

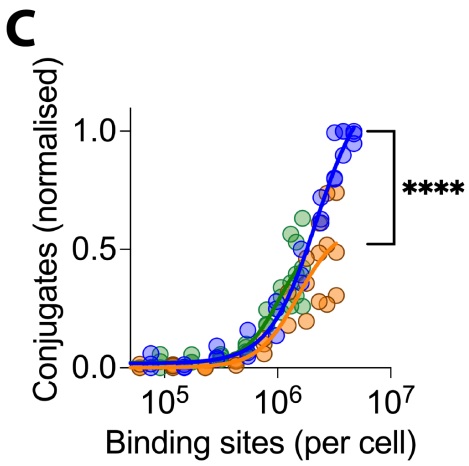

F Test	P value
CD80 vs CD43	<0.0001
CD80 vs CD52	0.5101
CD43 vs CD52	0.1139

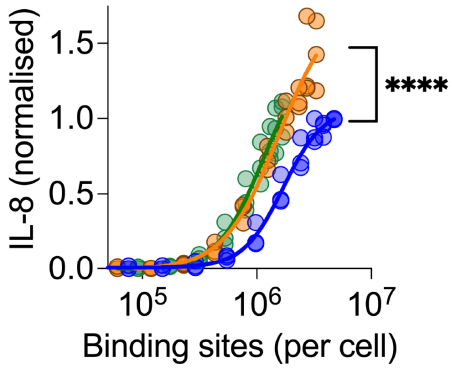

F Test	P value
CD80 vs CD43	<0.0001
CD80 vs CD52	<0.0001
CD43 vs CD52	0.4320

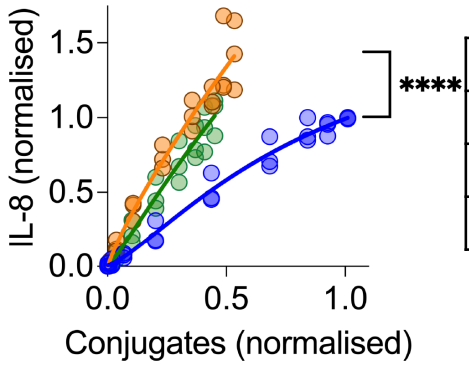

F Test	P value
CD80 vs CD43	<0.0001
CD80 vs CD52	<0.0001
CD43 vs CD52	<0.0001

Figure 4

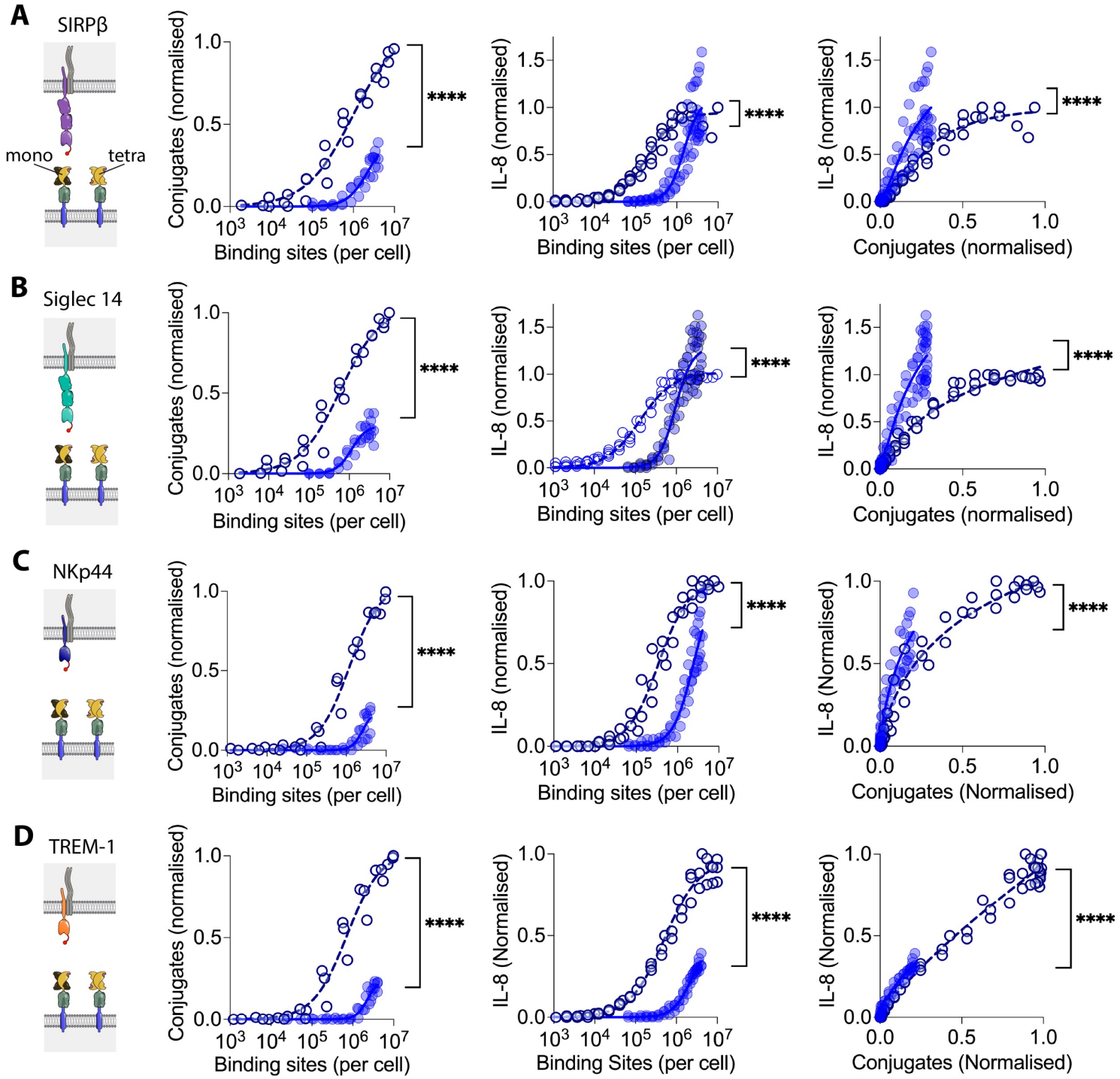
A
SIRPβ
mono
tetra
Conjugates (normalised)
Binding sites (per cell)
IL-8 (normalised)
Conjugates (normalised)
****
B
Siglec 14
C
NKp44
IL-8 (Normalised)
Conjugates (Normalised)
D
TREM-1
Binding Sites (per cell)

Figure 5

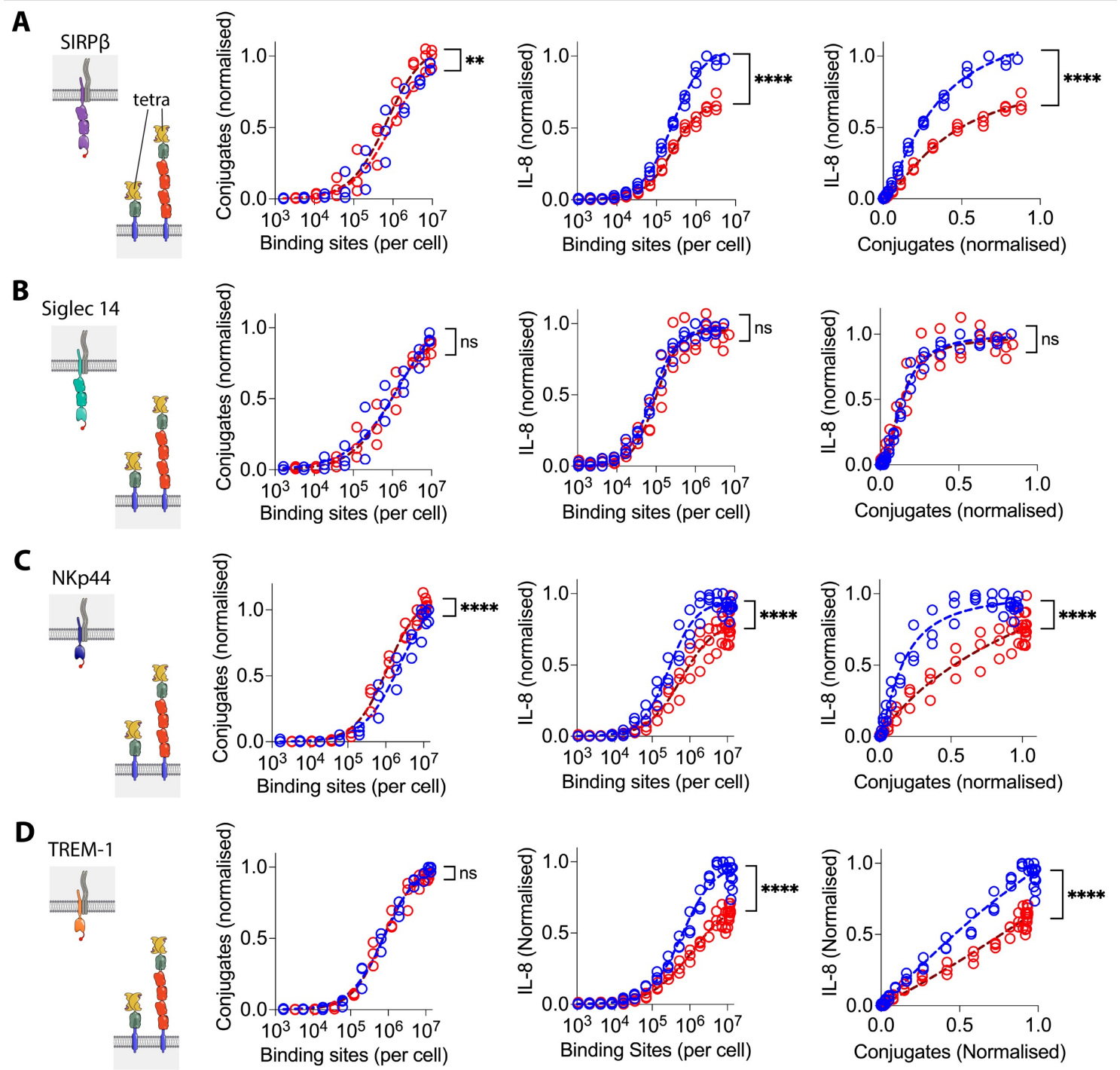
A
SIRPβ
tetra
Conjugates (normalised)
Binding sites (per cell)
**
IL-8 (normalised)
Binding sites (per cell)
****
IL-8 (normalised)
Conjugates (normalised)
****
B
Siglec 14
Conjugates (normalised)
Binding sites (per cell)
ns
IL-8 (normalised)
Binding sites (per cell)
ns
IL-8 (normalised)
Conjugates (normalised)
ns
C
NKp44
Conjugates (normalised)
Binding sites (per cell)
****
IL-8 (normalised)
Binding sites (per cell)
****
IL-8 (normalised)
Conjugates (normalised)
****
D
TREM-1
Conjugates (normalised)
Binding sites (per cell)
ns
IL-8 (Normalised)
Binding Sites (per cell)
****
IL-8 (Normalised)
Conjugates (Normalised)
****

sFigure 1

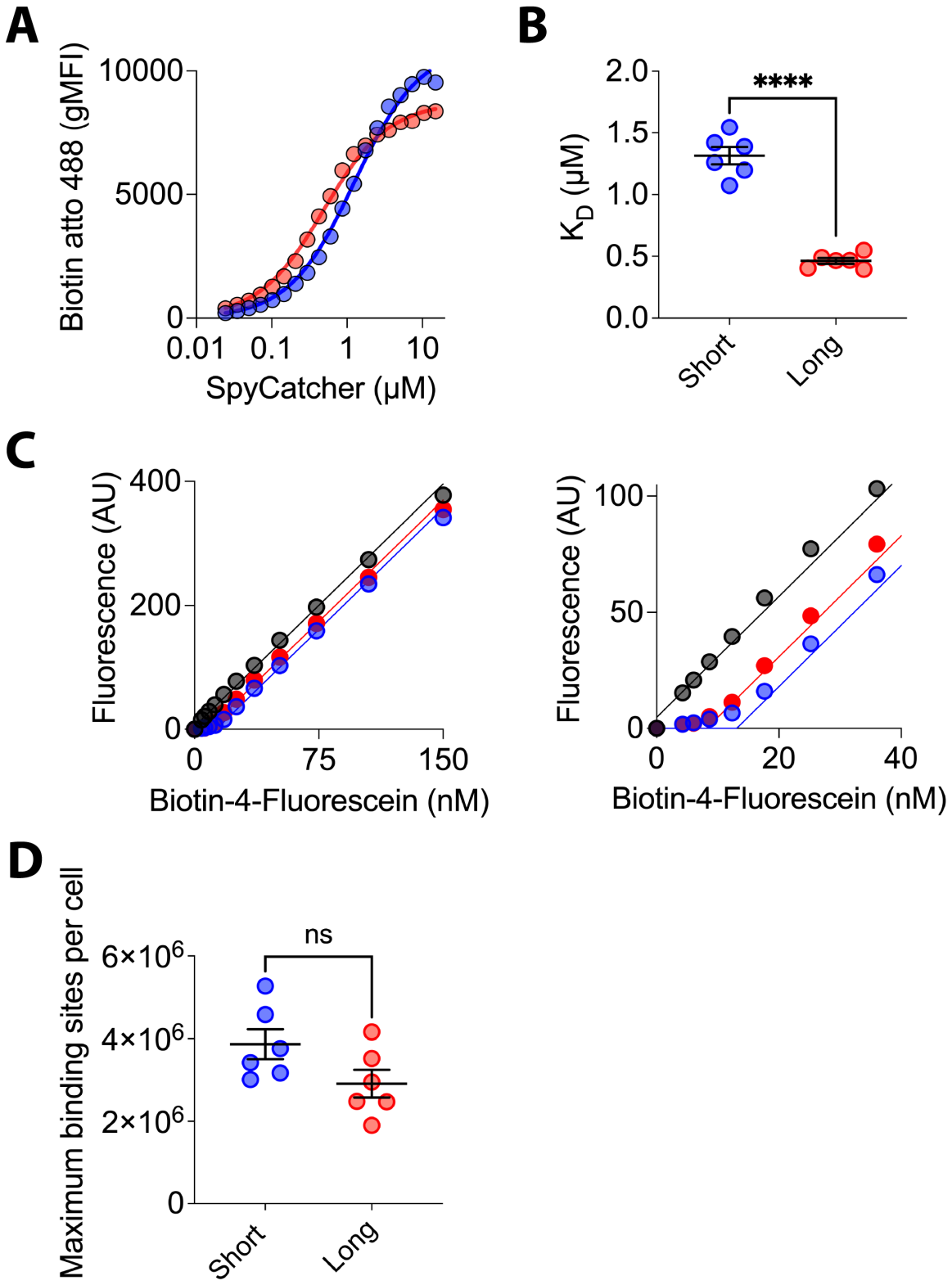
A
Biotin atto 488 (gMFI)
10000
5000
0
0.01
0.1
1
10
SpyCatcher (μM)
B
K_D (μM)
2.0
1.5
1.0
0.5
0.0
****
Short
Long
C
Fluorescence (AU)
400
200
0
0
75
150
Biotin-4-Fluorescein (nM)
Fluorescence (AU)
100
50
0
0
20
40
Biotin-4-Fluorescein (nM)
D
Maximum binding sites per cell
6×10^6
4×10^6
2×10^6
0
ns
Short
Long

sFigure 2

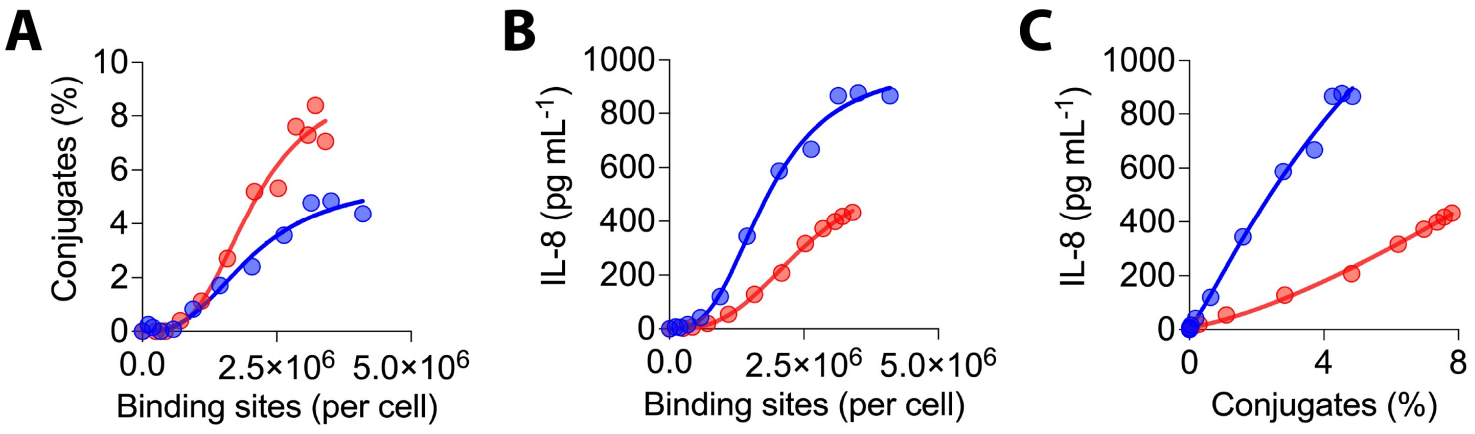
A
Conjugates (%)
10
8
6
4
2
0
0.0
2.5×10^6
5.0×10^6
Binding sites (per cell)
B
IL-8 (pg mL^-1)
1000
800
600
400
200
0
0.0
2.5×10^6
5.0×10^6
Binding sites (per cell)
C
IL-8 (pg mL^-1)
1000
800
600
400
200
0
0
4
8
Conjugates (%)

sFigure 3

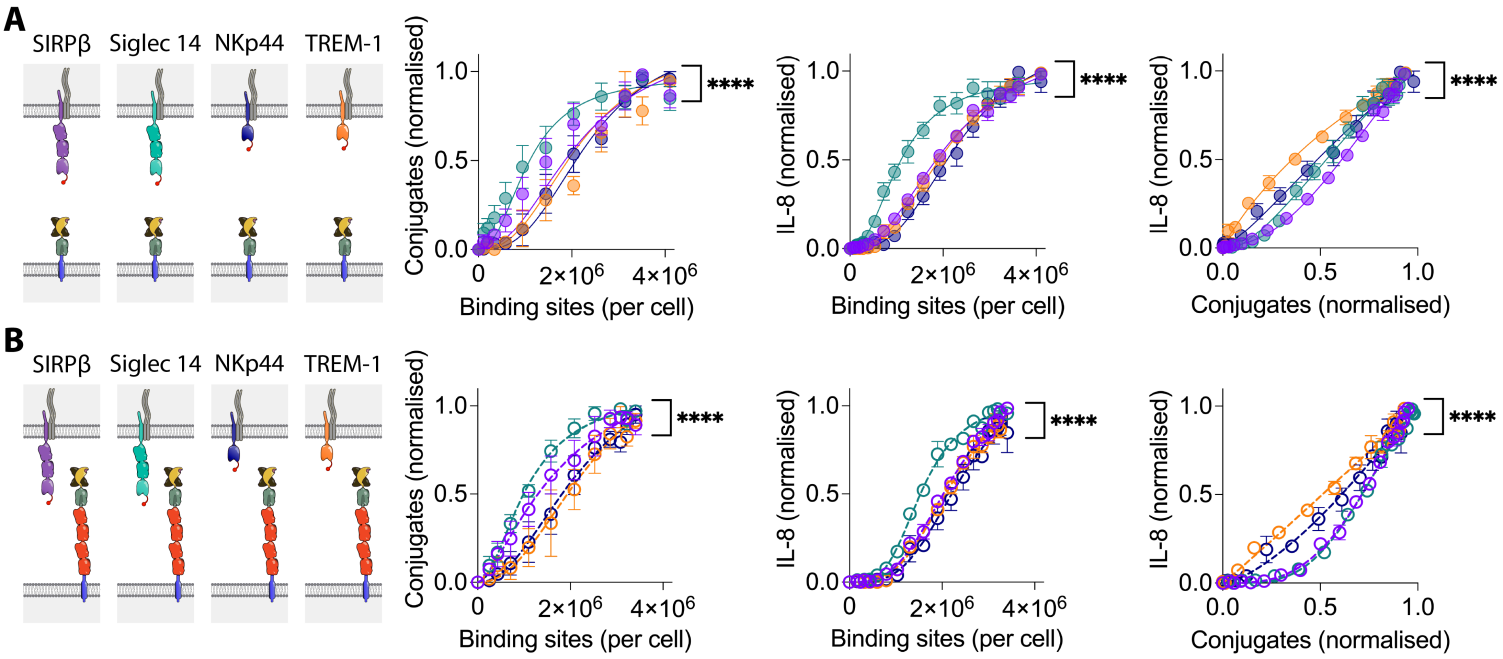

F Test	P value
SIRPß1 vs Siglec 14	0.0443
SIRPß1 vs NKp44	<0.0001
SIRPß1 vs TREM-1	<0.0001
Siglec 14 vs NKp44	<0.0001
Siglec 14 vs TREM-1	<0.0001
NKp44 vs TREM-1	0.4043

F Test	P value
SIRPß1 vs Siglec 14	<0.0001
SIRPß1 vs NKp44	0.0699
SIRPß1 vs TREM-1	<0.0001
Siglec 14 vs NKp44	<0.0001
Siglec 14 vs TREM-1	<0.0001
NKp44 vs TREM-1	0.0055

F Test	P value
SIRPß1 vs Siglec 14	<0.0001
SIRPß1 vs NKp44	<0.0001
SIRPß1 vs TREM-1	<0.0001
Siglec 14 vs NKp44	<0.0001
Siglec 14 vs TREM-1	<0.0001
NKp44 vs TREM-1	<0.0001

F Test	P value
SIRPß1 vs Siglec 14	0.0084
SIRPß1 vs NKp44	<0.0001
SIRPß1 vs TREM-1	<0.0001
Siglec 14 vs NKp44	<0.0001
Siglec 14 vs TREM-1	<0.0001
NKp44 vs TREM-1	0.5775

F Test	P value
SIRPß1 vs Siglec 14	<0.0001
SIRPß1 vs NKp44	0.0873
SIRPß1 vs TREM-1	<0.0001
Siglec 14 vs NKp44	<0.0001
Siglec 14 vs TREM-1	<0.0001
NKp44 vs TREM-1	0.0467

F Test	P value
SIRPß1 vs Siglec 14	0.0036
SIRPß1 vs NKp44	<0.0001
SIRPß1 vs TREM-1	<0.0001
Siglec 14 vs NKp44	<0.0001
Siglec 14 vs TREM-1	<0.0001
NKp44 vs TREM-1	0.0004

sFigure 4

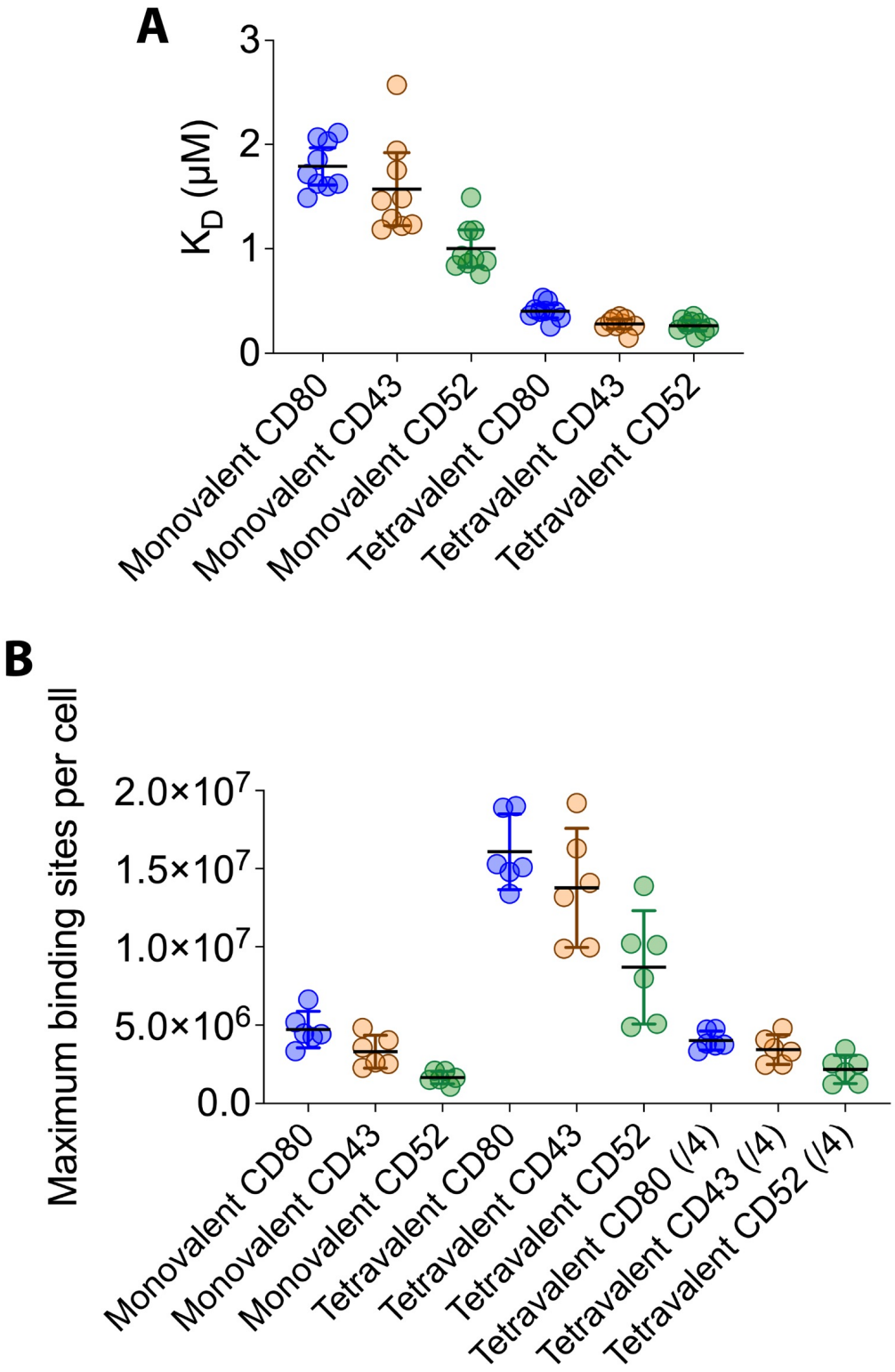
A
K_D (μM)
3
2
1
0
Monovalent CD80
Monovalent CD43
Monovalent CD52
Tetravalent CD80
Tetravalent CD43
Tetravalent CD52
B
Maximum binding sites per cell
2.0×10^7
1.5×10^7
1.0×10^7
5.0×10^6
0.0
Monovalent CD80
Monovalent CD43
Monovalent CD52
Tetravalent CD80
Tetravalent CD43
Tetravalent CD52
Tetravalent CD80 (/4)
Tetravalent CD43 (/4)
Tetravalent CD52 (/4)

sFigure 5

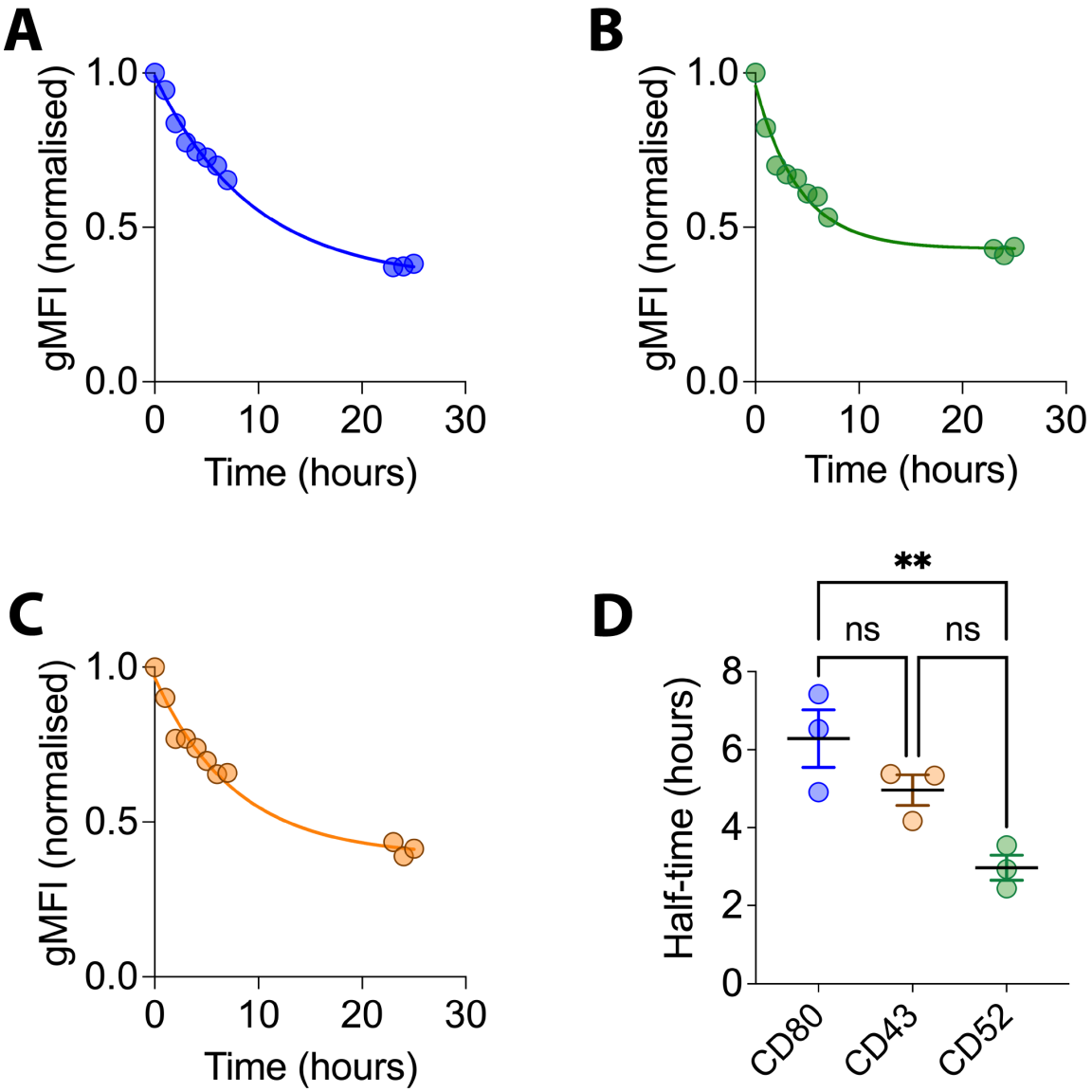
A
gMFI (normalised)
1.0
0.5
0.0
0
10
20
30
Time (hours)
B
gMFI (normalised)
1.0
0.5
0.0
0
10
20
30
Time (hours)
C
gMFI (normalised)
1.0
0.5
0.0
0
10
20
30
Time (hours)
D
**
ns
ns
Half-time (hours)
8
6
4
2
0
CD80
CD43
CD52

sFigure 6

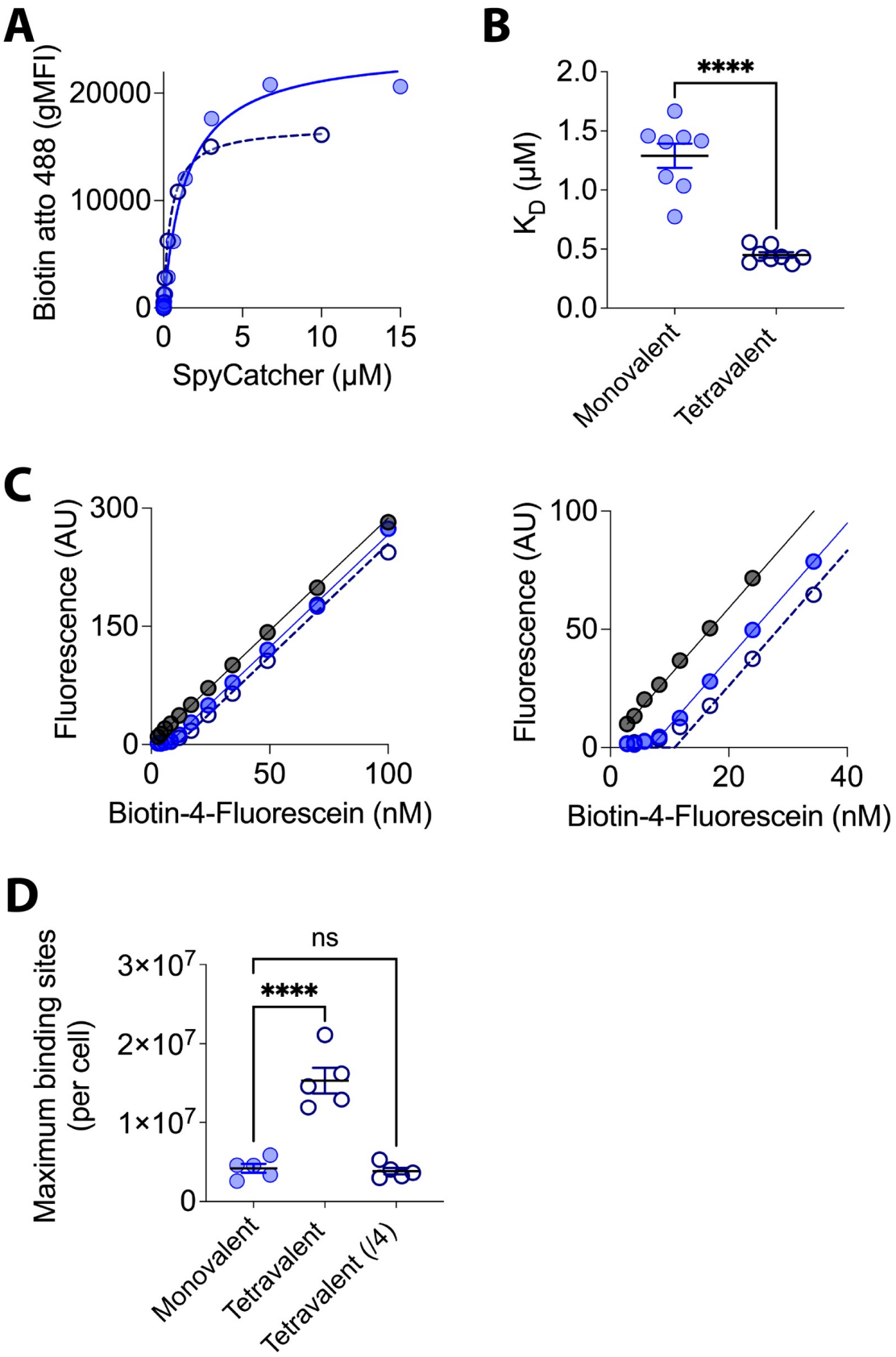
A
Biotin atto 488 (gMFI)
20000
10000
0
0
5
10
15
SpyCatcher (μM)
B
****
2.0
1.5
1.0
0.5
0.0
K_D (μM)
Monovalent
Tetravalent
C
Fluorescence (AU)
300
150
0
0
50
100
Biotin-4-Fluorescein (nM)
Fluorescence (AU)
100
50
0
0
20
40
Biotin-4-Fluorescein (nM)
D
Maximum binding sites (per cell)
ns
****
3×10^7
2×10^7
1×10^7
0
Monovalent
Tetravalent
Tetravalent (/4)

sFigure 7

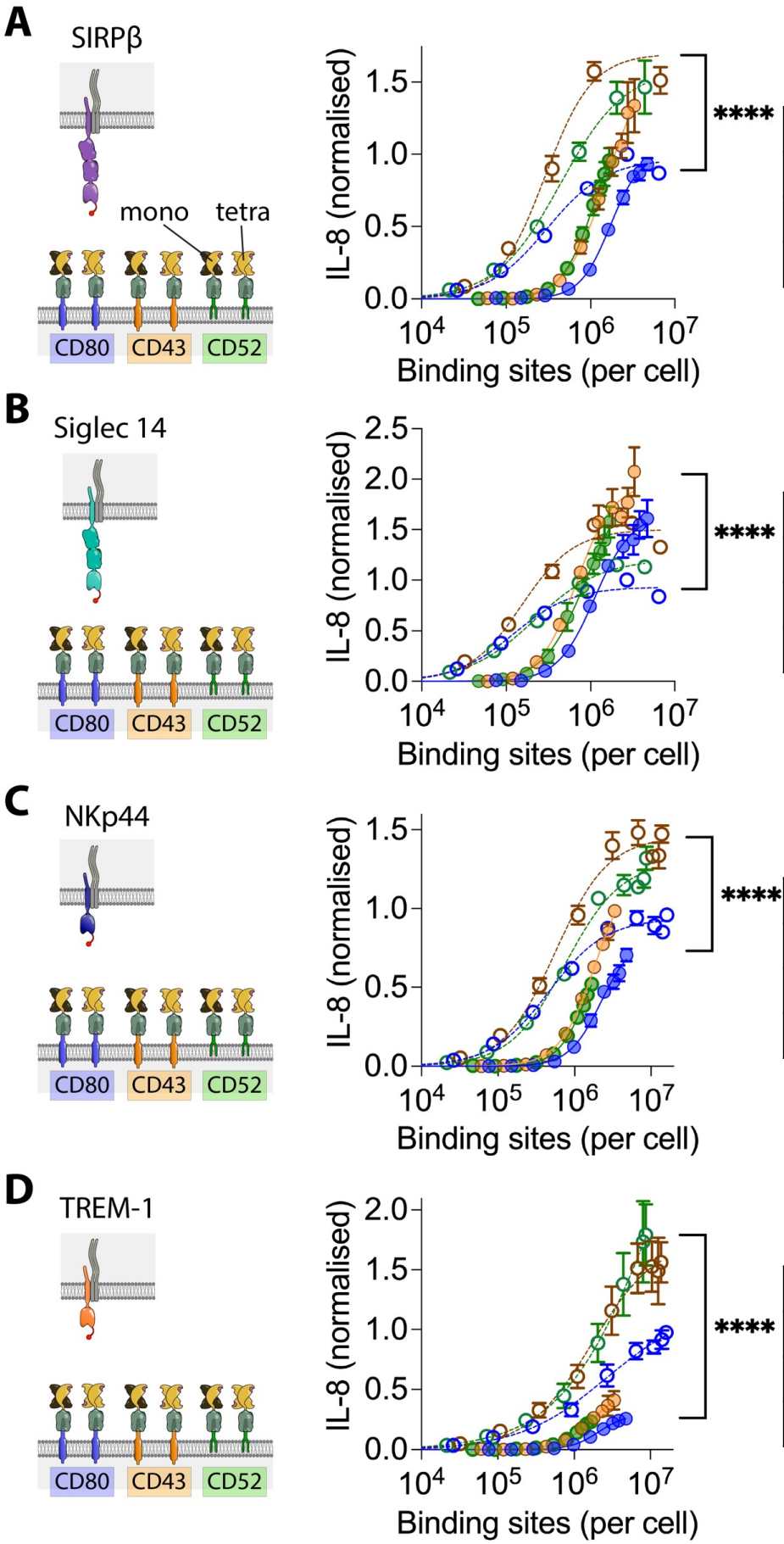

F Test	P value
CD80	<0.0001
CD43	<0.0001
CD52	<0.0001

F Test	P value
CD80	<0.0001
CD43	<0.0001
CD52	<0.0001

F Test	P value
CD80	<0.0001
CD43	<0.0001
CD52	<0.0001

F Test	P value
CD80	<0.0001
CD43	<0.0001
CD52	<0.0001

sFigure 8

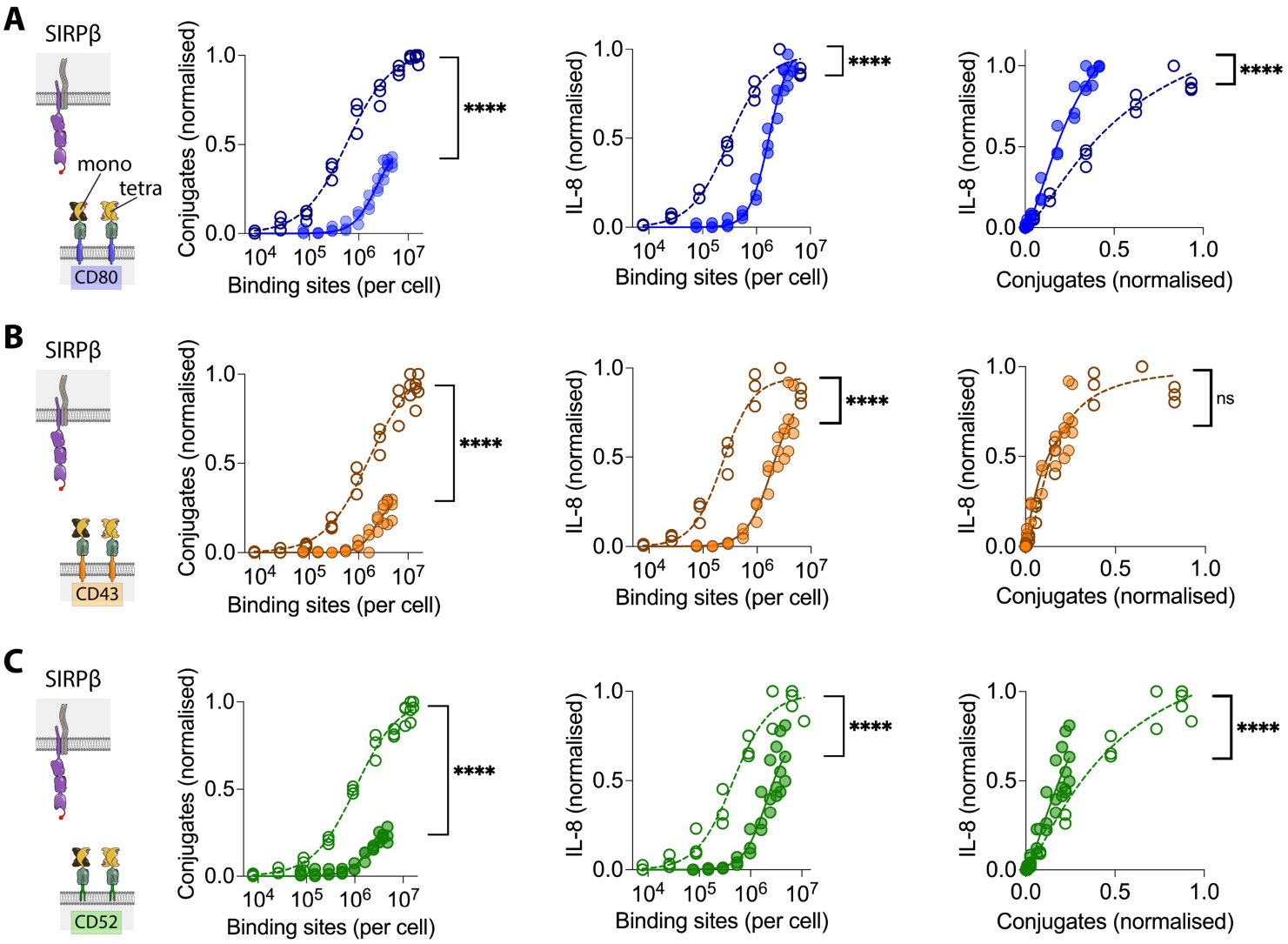
A
SIRPβ
mono
tetra
CD80
Conjugates (normalised)
Binding sites (per cell)
IL-8 (normalised)
Conjugates (normalised)
****
B
SIRPβ
CD43
ns
C
SIRPβ
CD52

sFigure 9

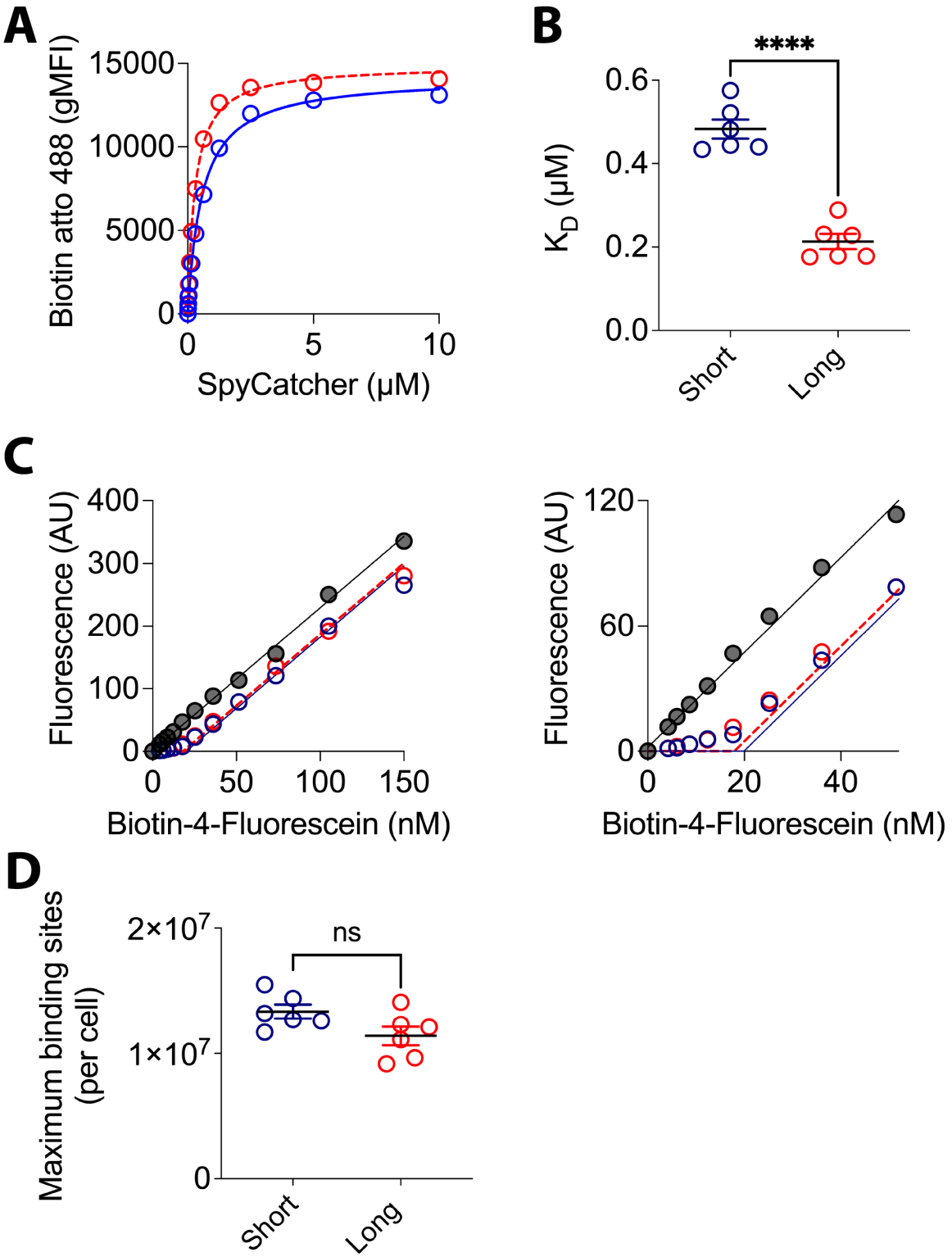
A
Biotin atto 488 (gMFI)
15000
10000
5000
0
0
5
10
SpyCatcher (μM)
B
****
K_D (μM)
0.6
0.4
0.2
0.0
Short
Long
C
Fluorescence (AU)
400
300
200
100
0
0
50
100
150
Biotin-4-Fluorescein (nM)
Fluorescence (AU)
120
60
0
0
20
40
Biotin-4-Fluorescein (nM)
D
Maximum binding sites (per cell)
2×10^7
1×10^7
0
ns
Short
Long